Jorge André Almeida Barreto

Licenciado em Ciências de Engenharia Física

Gas Gap Heat Switch for CryoFree Project

Dissertação para obtenção do Grau de
Mestre em Engenharia Física

Orientadora: Maria Isabel Simões Catarino, Prof.Auxiliar,
Universidade Nova de Lisboa

Júri:

Presidente:	Doutor José Paulo Moreira Santos
Arguente:	Mestre Soumen Kar
Vogal:	Doutora Maria Isabel Simões Catarino

FACULDADE DE
CIÊNCIAS E TECNOLOGIA
UNIVERSIDADE NOVA DE LISBOA

Setembro, 2014

Gas Gap Heat Switch for CryoFree Project

ACKNOWLEDGEMENTS

Aproveito nesta página para expressar todos os meus agradecimentos a algumas pessoas que me apoiaram ao longo desta luta.

Começo por agradecer à minha orientadora, Profª Isabel Catarino, pela oportunidade de realizar este projeto, todo o tempo disponibilizado e apoio dado ao longo desta dissertação.

Também quero agradecer ao Profº Grégoire Bonfait, sempre que possível disponibilizou o seu tempo para troca de ideias.

Agradeço também aos meus colegas de laboratório: Patrícia e Gonçalo pela paciência e disponibilidade na resolução de qualquer assunto durante o semestre.

Agradeço à metalomecânica *A. M. Tita, Lda.* pela disponibilidade na construção das peças.

Agradeço às oficinas do Departamento de Física, especialmente ao Faustino, pela sua assistência ao longo do projeto.

Agradeço à Sara, do Departamento de Conservação e Restauro, pelo seu tempo dedicado na obtenção de imagens de raios X.

Agradeço ainda à Fundação para Ciência e Tecnologia pela bolsa de iniciação científica atribuída, ao abrigo do projeto "Gestão térmica de fonte fria sem fluidos criogénicos", com a referência PTDC/EMS-PRO/1065/2012.

Por último, mas com maior importância, agradeço à minha família por me ter concedido a oportunidade de realizar este curso e todo o apoio incondicional que me deram ao longo destes 5 anos e também aos meus amigos e colegas que me acompanharam nesta caminhada, sem vós teria sido bastante difícil chegar ao fim.

Muito obrigado a todos

ABSTRACT

Cryogen-free superconducting magnet systems have become popular during the last two decades for the simple reason that with the use of liquid helium is rather cumbersome and is a scarce resource.

Some available CFMS uses a mechanical cryocooler as cold source of the superconductor magnet. However, the cooling of the sample holder is still made through an open circuit of helium.

A thermal management of a completely cryogen-free system is possible to be implemented by using a controlled gas gap heat switch (GGHS) between the cryocooler and the variable temperature insert (VTI). This way it would eliminate the helium open circuit.

Heat switches are devices that allow to toggle between two distinct thermal states (ON and OFF state). Several cryogenic applications need good thermal contact and a good thermal insulation at different stages of operation.

A versatile GGHS was designed and built with a 100 μm gap and tested with helium as exchange gas. An analytic thermal model was developed and a good agreement with the experimental data was obtained.

The device was tested on a crycooler at 4 to 80 K ranges. A 285 mW/K thermal conductance was measured at ON state and 0.09 mW/K at OFF. 3000 ON/OFF thermal conductance ratio was obtained at 4 K with helium.

Keywords: Cryogenics, Heat switch, Adsorption, Cryofree

RESUMO

Os sistemas de medição de propriedades magnéticas livres de líquidos criogénicos em circuito aberto têm sido populares nas últimas duas décadas devido à escassez de hélio liquido.

Alguns destes sistemas usam um criorrefrigerador como fonte fria do magneto supercondutor. No entanto, o arrefecimento do porta amostras ainda é feito através de circulação de hélio.

Um controlo térmico de um sistema livre de líquidos em circuito aberto é possível através da inclusão de um interruptor térmico com hiato a gás de troca entre o criorrefrigerador e o porta amostras.

Estes interruptores são dispositivos que permitem comutar entre dois estados de condução térmica distintos (estados ON e OFF). Várias aplicações criogénicas necessitam de um bom contacto térmico e de uma boa insulação térmica em diferentes fases do processo.

Foi desenhado, construído e testado um interruptor térmico com um hiato de 100 μm e testado com hélio como gás de troca. Foi desenvolvido um modelo analítico que mostrou ter boa concordância com os resultados obtidos.

O dispositivo foi testado num criorrefrigerador entre 4 e 80 K. Uma condutância de 285 mW/K foi obtida para estado ON e 0.09 mW/K no OFF. Uma razão de condutância térmica ON/OFF de 3000 foi obtida a 4 K para o gás de hélio.

Palavras-chave: Criogenia, Interruptor térmico, Adsorção, Cryofree

Contents

List of Figures

CHAPTER 1

INTRODUCTION

Strong magnetic fields are achieved by using electromagnets, coils circulated by electric current. A 10 Tesla magnetic field is common. Reaching such field implies currents about 100 Ampere. The Joule heating and power consumption on a metallic wire is huge so that the superconducting wire is usually preferred for the coil. This way there is no dissipation as long as the material is kept below a critical temperature to remain at its superconductor state. The production of such field requires maintenance and control of low temperatures.

Typically the low temperature superconducting wires are made of niobium alloys and cooled down by a liquid helium bath (4 K). Liquid helium is not only expensive but is also a very limited resource. The recent developments of reliable cryocoolers with some cooling power at 4 K along with the environmental resources issues lead to a trend of substitution of liquid helium baths for cryocoolers as a cold source.

The superconducting coil can be cooled down by a cryocoler with the advantage of autonomy. The same cooler can also be used in parallel for cooling down a sample holder for measurements of magnetic properties, as long as the cooling power that is diverted from the coil doesn't put in risk the superconducting coil returning to its normal state (resistive). Some "cryogen-free" systems with a variable temperature insert (VTI) along with a cryocooler are now available, but they are not exactly cryogen-free, because these systems are still using a helium flow to the sample. A thermal management of such system is possible to be implemented by using a controlled heat switch between the cryocooler and the VTI. This way it would eliminate the open circuit helium. This was the main work of this dissertation.

A heat switch is a device that allows toggling between states of high and low thermal conductance. One of the most popular forms of a heat switch is the gas gap one. In a gas gap heat switch (GGHS) the thermal connection depends on the presence (ON state) or the absence of gas (OFF state) in the narrow gap existent between two blocks. The heat conduction is made through the gas in the ON state (i.e viscous regime) and at the OFF

state (i.e molecular regime), being the conduction through the gas at this state insignificant.

The amount of gas in a GGHS can be managed by using an external pump and a gas reservoir. Or it can be managed by using the sorption properties of an activated charcoal and benefit from a compact and small closed system. This way the actuation of the heat switch is made upon the heating/cooling of a cryopump.

The prediction and planning of the thermal behaviour of the switch is made upon knowledge of the sorption's properties of the activated charcoal. The main goal is to develop a thermal architecture for a versatile use of one cryocooler that cools down a superconductor coil and a variable temperature insert (VTI). For that, it will be used a gas gap heat switch to cool down the VTI in parallel with the superconducting coil. The inclusion of this heat switch allows the opening of the sample holder without warming up the coil (preventing the quench).

The case study relies on a concrete problem of a 4 K, 6 T cryostat with a VTI that is aimed to be implemented at Inter University Accelerator Centre (IUAC), at New Delhi India, for measurements of magnetic properties [1].

A prototype of a gas gap heat switch was designed, built and characterized in this work, this prototype requirements obey to the IUAC's specifications.

In this dissertation the operation of heat switches is presented in Chapter 2, the thermal conduction in gases and solids is presented in Chapter 3, the designed prototype is presented in Chapter 4, the experimental setup is presented in Chapter 5 and the results with the respective discussion are presented in Chapter 6.

CHAPTER 2

HEAT SWITCHES

Heat switches, known also as thermal switches, are devices that allow to toggle between two distinct thermal states: an ON state, good thermal conduction; and an OFF state, with poor thermal conduction. When a switch is installed in the heat conduction path, the change in thermal conductance can control the temperature of the coupled component. Heat switches can passively control the temperature of electronic components or instrumentation without the use of thermostats and heaters, thereby reducing power requirements.

Cryogenic applications use heat switches to minimize heat loads on cooling systems by disconnecting components when cooling is not required or disconnecting redundant refrigerators that are not providing cooling or because they have failed or been turned off.

The heat switches are developed according to their applications. Each type is based on different physical principles, ON/OFF thermal conductance ratio, working temperature, also their weight and size and moving parts.

The typical heat switches are:

Mechanical Heat conduction is assured by the physical contact between two plates. Usually the switching is achieved by mechanical action, thermal action or electromagnetic.

Fluid-loop Thermal commutation is achieved by the variation of a fluid's flux in a closed loop.

Gas-gap Thermal switching is obtained by the presence or absence of gas in the narrow gap space existent between two blocks.

2.1 Gas gap heat switch

The simplest and most commonly used method of thermally connecting the various parts of a cryogenic apparatus is the gas gap heat switch. These switches are controlled by the gas pressure in the existent narrow gap between two blocks. Usually high thermal conductivity materials are used for the blocks (e.g copper, beryllium...). A supporting shell encloses the gas and supports mechanically these two blocks. This shell should minimize the thermal short-circuit between the blocks and should have a thin wall with a low thermal conductivity material (e.g titanium, stainless steel...), the selected material must also have a good rigidity (Fig.2.1).

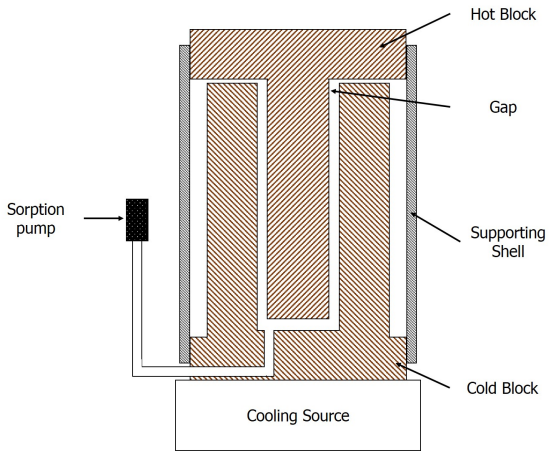

Figure 2.1: General scheme of a gas-gap heat switch.

The presence of enough gas inside the heat switch allows a good conduction between blocks, corresponding to the ON state. A low gas pressure results in a poor heat flux through the gap, in a first approximation the heat only passes through the shell, corresponding to the OFF state.

In the ON state, the thermal conductance is pressure independent, inversely to the length of the gap and proportional to the exchange surface between blocks (Sec.3.2). On the other hand, given the absence of gas inside the heat switch, the OFF thermal conductance depends only on the low thermal conductivity material that holds the blocks, since all heat goes through this material.

The management of the gas inside the switch could be assured by a feeding mechanism and an external pump (inducing vibrations) or it can be managed by using the sorption properties of an activated charcoal and benefit from a compact and small closed system. This way the actuation of the heat switch is made upon the heating/cooling of a cryopump.

However, their operational temperature range is limited by the gas-sorbent pair adsorption characteristics. The gas gap heat switches are customizable, because the same device can work with different gases, corresponding to different settings for both ON and OFF onsets.

2.2 Applications

The operation of space instruments (e.g infrared sensors) requires cryogenic temperatures. Maintenance of these temperatures depends on heavy cooling systems, many of which utilize mechanical cryocoolers that must be redundant for high reliability. Unfortunately, when a redundant cryocooler is connected to a system but not used, it introduces a large parasitic heat load. A heat switch can significantly improve this situation by thermally disconnecting the backup cryocooler from the system when it is not in use. This disconnect is accomplished by the insertion of a heat switch between each cryocooler and the cold load (see Fig.2.2).

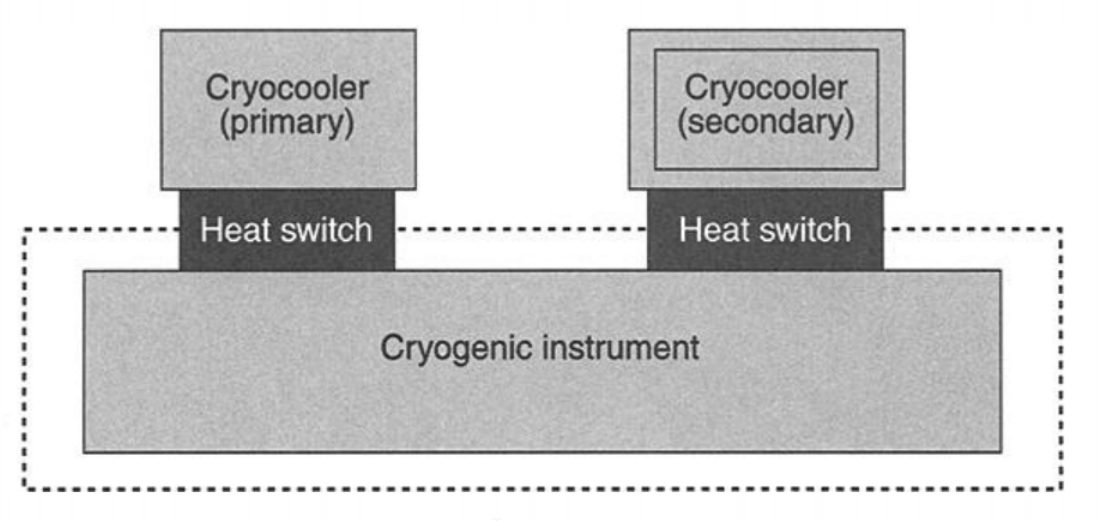

Figure 2.2: Cryocooler application [2].

When the cryocooler is turned on, the heat switch should not limit the available cooling power. On the other hand when it is disconnected it is necessary to have a good thermal decoupling, otherwise an unnecessary parasitical heat load is inserted into the system.

Marland [3] developed a thermal switch which main application was to couple redundant cryocoolers to a cryogenic component with minimal parasitic heat load from the non-operating cryocooler. .

Low temperature quiet environments are often necessary in many space technologies, the cooling without vibrations and electromagnetic noise induced by the compressor. In some cases the cryocooler vibrations can be incompatible with very high precision measurements. A solution to this problem would be to stop the cryocooler during the measurements, however this would lead to a rapid temperature increase. To avoid this temperature drift, it is possible to use thermal energy storage unit (ESU) that allows maintaining low temperature after the cryocooler stooping. This acts as a temporary compact cold source in a completely vibration-free environment. An ESU consists in an "enthalpy reservoir" coupled by a heat switch to the cryocooler cold finger (see Fig.2.3).

In the first phase, this reservoir is cooled down by the cryocooler through the heat

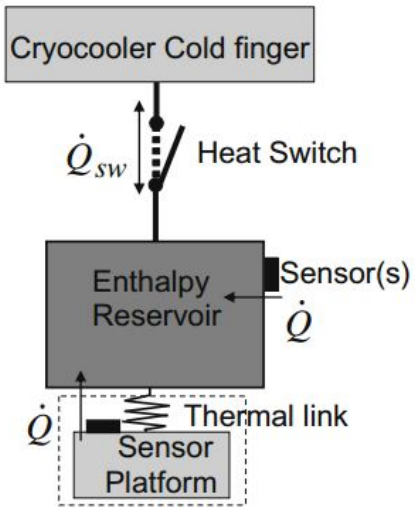

Figure 2.3: General scheme of the ESU thermally coupled to cryocooler cold finger by a heat switch [4].

switch (highly conducting state). In the second phase, the heat switch is opened (OFF state) leading to a thermal decoupling between the cryocooler and the enthalpy reservoir. Due to its high heat capacity or due to its latent heat, the temperature of the reservoir rises really slowly and a vibration-free with no electromagnetic noise cold source is obtained.

An ESU capable of storing 36 Joules between 11 and 20 K is described at [4]. The tests showed that a platform can be stabilized at 19 K during more than 1 h using this ESU. In reference [5] is shown a 36 Joules ESU between 3 and 6 K. A stable 6 K temperature was maintained during more than 50 min in a completely silent environment.

2.3 Target application

The problem under research concerns the cooling down and maintenance of a cryostat equipped with a superconducting coil and a variable temperature insert (VTI), as schematized in Fig.2.4. The VTI holds the sample and the measurement instrument. The superconductor is normally kept at about 4 K while the VTI shall swap from 4 K up to room temperature. Traditionally the cooling of such system is done by a liquid helium bath. Keeping a liquid bath is expensive and the lack of helium is turning on an environmental issue also [6]. The idea is to completely replace the circulating helium, by using a cryocooler that serves as a parallel cold source. Such cold source would serve primarily the superconducting coil which can never surpass the critical temperature (4 K in this case). If the temperature of the superconductor rises above this value, it risks losing its properties by getting resistive and the subsequent Joule heating may get disastrous, known as *quench*. Secondarily the same cold source can use the remnant cooling power for the VTI. The diverting of the cooling power is intended to be made via a gas gap heat switch which

actuation is made with a cryopump. Such cryopump adsorbs gas when cooled down opening the switch and releases gas when warmed up, closing the switch.

The problem was put by the IUAC laboratory (New Delhi) and it is interesting for the implementation of a completely closed cycle cryogenic system for a general purpose superconducting magnetic facilities namely for the magnetic resonance scanning. A closed cycle cryogenic system provides autonomy of the system as long as the electric power exists. Some off-the-shelf "croyogen-free" systems are already available. Nevertheless, when those systems include a VTI they include a flow of helium in an open circuit. The construction and implementation of a heat switch at this system will vanish the helium bath, making this system completely "croyogen-free".

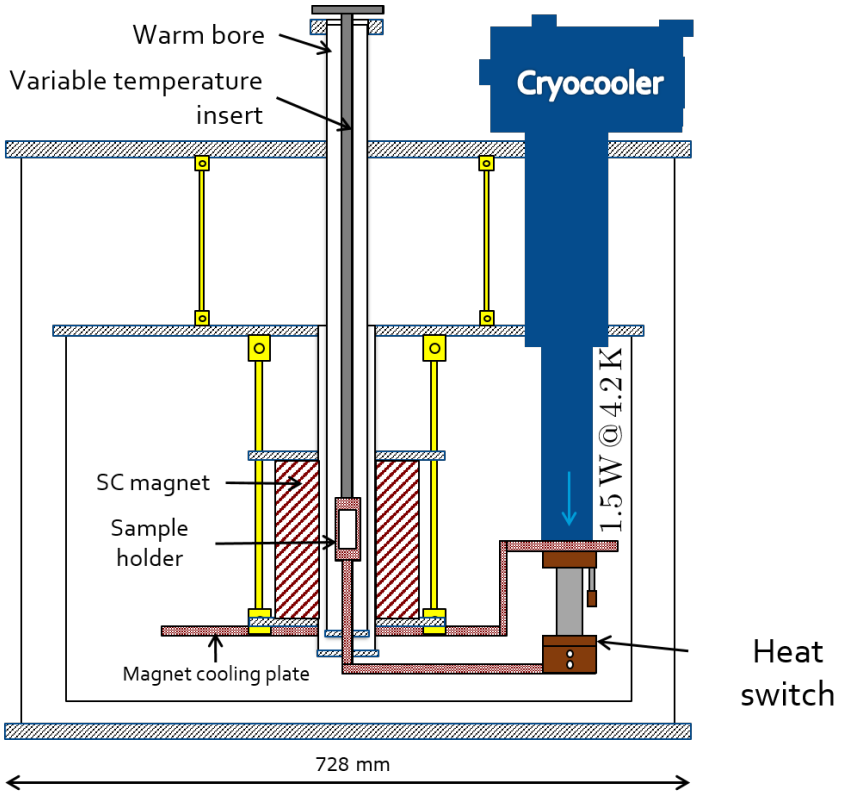

Figure 2.4: Scheme of the magnet cryostat at Inter University Accelerator Centre (IUAC) New Delhi.

CHAPTER 3

THERMAL MODEL

This chapter describes the thermal conductivity of gases and solids and its importance in design of a GGHS.

3.1 Heat transfer

Heat transfer consists on the exchange of thermal energy between physical systems at different temperatures. The rate of energy transfer may depend both on temperature and pressure. The fundamental modes of heat transfer are conduction, convection, and radiation.

Convection is heat transfer by mass motion of a fluid such as gases or liquids when the heated fluid is caused to move away from the source of heat, carrying energy with it.

Radiation is a method of heat transfer that does not rely upon any contact between the heat source and the heated object as is the case with conduction and convection. Heat can be transmitted though vacuum by thermal radiation. This is a electromagnetic radiation where no mass is exchanged and no medium is required in the process of radiation. All objects with a temperature greater than absolute zero emits thermal radiation.

Heat transfer by conduction is greatly described, due to its importance on the thermal conductance of heat switches.

Consider a cylindrical rod of a material (solid, liquid or gaseous) with its end faces maintained at different temperatures, $T_1 > T_2$. The temperature difference causes conduction heat transfer in the positive x direction, as shown in Fig.3.1.

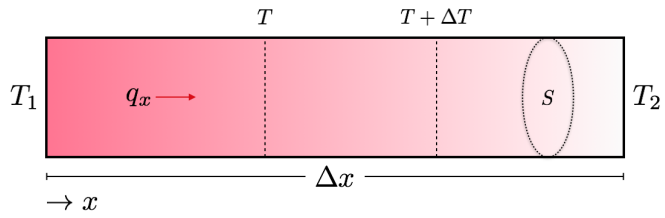

Figure 3.1: Steady-state heat conduction.

The differential form of Fourier's Law of thermal conduction shows that the local heat flux density, $\vec{q}$, is equal to the product of thermal conductivity, k, and the negative temperature gradient, $-\vec{\nabla}T$. The heat flux density is the amount of energy that flows through a unit area per unit time.

$$\vec{q} = -k\vec{\nabla}T \tag{3.1}$$

where (considering the SI units), k is the material's thermal conductivity, $\mathrm{W.m^{-1}.K^{-1}}$ and $\vec{\nabla}T$ is the temperature gradient, $\mathrm{K.m^{-1}}$. The minus sign is necessary because heat is always transferred in the direction of the decreasing temperature. For many simple applications, Fourier's Law is used in its one-dimensional form. In the x-direction (e.g. Fig.3.1).

$$q_x = -k\frac{dT}{dx} \tag{3.2}$$

From kinetic theory of gases it is possible to obtain an approximation of the thermal conductivity. This coefficient express the ability of the material to conduct heat. In the example given above, Fig.3.1, consider a slice of this rod with section S and length λ[1] and a temperature difference ΔT between its ends. The number of particles between $T + \Delta T$ and T is:

$$N = n\lambda S \tag{3.3}$$

where n is the particle density (number of particles per volume unit), S is the cross section. The number of particles in the positive x direction with mean velocity $\overline{v_x}$ is,

$$N^+ = \frac{1}{2}n\overline{v_x}\tau S \tag{3.4}$$

where τ is the mean free time (time between collisions). Thus, the rate of transfer of particles through a unit area in the positive x direction is,

$$\Phi^+ = \frac{1}{2}n\overline{v_x} \tag{3.5}$$

[1] λ is the mean free path: average of the distances that a particle travels between collisions

Likewise, in the negative x direction the particle flux is,

$$\Phi^{-} = -\frac{1}{2} n\overline{v_x} \tag{3.6}$$

Consider the energy of each particle is his internal energy $\epsilon(T)$. Therefore, the energy flux in the positive x direction is,

$$\Phi_E^{+} = \frac{1}{2} n\overline{v_x}[\epsilon(T + \Delta T) - \epsilon(T)] \tag{3.7}$$

Expanding the term $\epsilon(T + \Delta T)$ from Eq.3.7 in a first order Taylor series comes $\epsilon(T) + \Delta T\, \mathrm{d}\epsilon(T)/\mathrm{d}T$, being the term $\mathrm{d}\epsilon(T)/\mathrm{d}T$ the specific heat of one particle. By definition, specific heat capacity c is the amount of heat required to change one mole of a substance by one degree in temperature. Then, Eq.3.7 can be expressed as,

$$\Phi_E^{+} = \frac{1}{2} cn\overline{v_x}\Delta T = \frac{1}{2}\overline{v_x} C\Delta T \tag{3.8}$$

where C is the specific heat per unit volume at constant volume ($C = c.n$).
As for the opposite direction, the energy flux is,

$$\Phi_E^{-} = -\frac{1}{2} n\overline{v_x}[\epsilon(T) - \epsilon(T + \Delta T)] = \frac{1}{2}\overline{v_x} C\Delta T \tag{3.9}$$

The heat flux density is given by the sum of Eqs.3.7 and 3.9.

$$q_x = \Phi_E^{+} + \Phi_E^{-} = \overline{v_x} C\Delta T \tag{3.10}$$

The temperature difference ΔT can be written as function of $\lambda = \overline{v_x}\tau$.

$$\Delta T = \frac{\mathrm{d}T}{\mathrm{d}x}\lambda = \frac{\mathrm{d}T}{\mathrm{d}x}\overline{v_x}\tau \tag{3.11}$$

Since the mean square speed is,

$$\overline{v^2} = \overline{v_x^2} + \overline{v_y^2} + \overline{v_z^2} \tag{3.12}$$

and if the particle flux is isotropic, the mean square speed is,

$$\overline{v_x^2} = \frac{1}{3}\overline{v^2} \tag{3.13}$$

Considering Eqs.3.11, 3.10 and 3.13, the heat flux is,

$$q_x = \frac{1}{3} C\,\overline{v}\,\lambda \frac{\mathrm{d}T}{\mathrm{d}x} \tag{3.14}$$

Comparing the previous equation with Eq.3.2 comes,

$$k = \frac{1}{3} C\,\overline{v}\,\lambda \tag{3.15}$$

The thermal conductivity is proportional to the specific heat per unit volume C, average gas velocity $\overline{v}$ and mean free path λ. This general equation works for any type of particles

(atoms, electrons). It is used as a first approximation of the thermal conductivity of different materials (solid, liquid or gaseous).

By integrating the differential form Eq.3.1 over the material's total surface A, we obtain the integral form of Fourier's law,

$$\dot{Q} = \frac{\partial Q}{\partial t} = -k \oint_A \vec{\nabla} T \cdot \vec{dS} \tag{3.16}$$

where $\partial Q/\partial t$ or $\dot{Q}$ is the amount of heat transferred per unit time (in W). When integrated for a homogeneous material of one dimension geometry between two endpoints at constant temperature like the cylindrical rod, the heat flow rate is,

$$\dot{Q} = -k\frac{S}{L}\Delta T \tag{3.17}$$

where L is the distance between the ends and S the cross-sectional surface area. However, this last equation is valid if k is approximately constant between T_1 and T_2 ($\Delta T = T_1 - T_2$).

From Eq.3.17 the following equation can be derived, as long as k is constant. Thermal resistance R is the reciprocal of thermal conductance K.

$$K = k\frac{S}{L} = \frac{1}{R} \tag{3.18}$$

Thus, Eq.3.17 written as function of thermal resistance R or thermal conductance K is:

$$\dot{Q} = -K\Delta T = -\frac{1}{R}\Delta T \tag{3.19}$$

The heat flow can be modelled by analogy to an electronic circuit, where the flow rate $\dot{Q}$ is represented by current, temperature by voltage and thermal resistance by resistance (e.g Fig4.3).

Meanwhile, at most situations k is not constant, it has a strong dependence on temperature (v increases with increasing temperature), then $k(T)$ must be integrated from T_1 to T_2.

$$\dot{Q} = \frac{S}{L}\int_{T_2}^{T_1} k(T)dT \tag{3.20}$$

An analytic solution of the integral from Eq.3.20 is not convenient to use. Its values for various materials between given temperatures are tabulated (see Annex 8.1).

3.2 Conduction in gases

The mean free path λ is the average distance traversed by a molecule between collisions. If the distance between collisions is small comparatively to the length of the system ($\lambda \ll \delta$) the gas flow is said to be viscous, when this distance is higher it is molecular ($\lambda \gg \delta$), or ballistic. At the viscous regime the gas particles collide with each other, making the heat transfer more effective (high conductance), since the hotter particles will transfer constantly energy to the colder ones, this is also called classical conduction.

At the molecular flow the particles basically collide with the walls, because they travel longer without colliding, this regime of conduction is unneffective (low conductance), Fig.3.2, depicts both modes of heat conduction in gases.

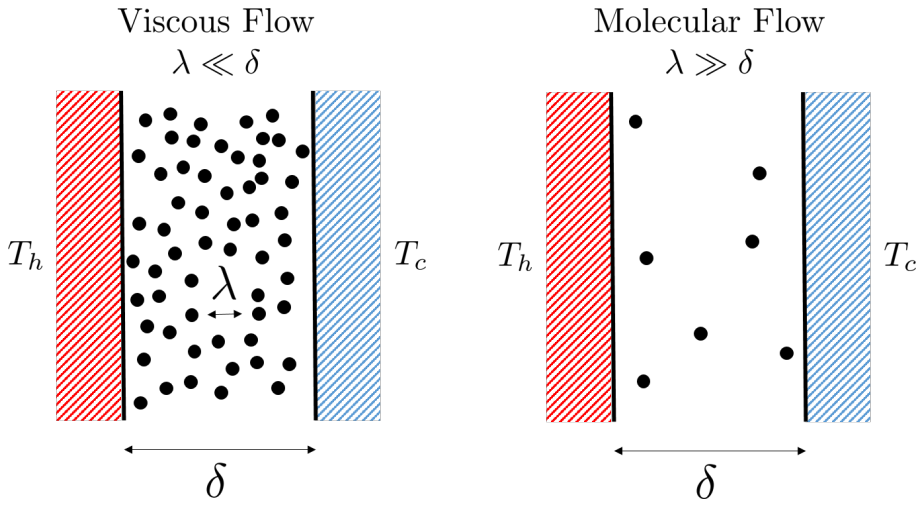

Figure 3.2: Comparison between viscous and molecular flow.

3.2.1 Viscous flow

From kinetic theory of gases, mean free path of a particle is:

$$\lambda = \frac{1}{n\sigma} \tag{3.21}$$

where n is the number of molecules per unit volume and σ the collisional cross section. For an ideal gas the free mean path is:

$$\lambda = \frac{RT}{N_A P}\frac{1}{\sigma} \tag{3.22}$$

The mean free path is proportional to temperature and inversely to pressure. Known the root-mean-square speed for an ideal gas:

$$v_{\text{rms}} = \sqrt{\frac{3RT}{M}} \tag{3.23}$$

Where M is the molar mass. This expression shows that, at a given temperature, lighter molecules move faster than do heavier molecules. Considering expression 3.15, the thermal conductivity for an ideal gas comes:

$$k = \frac{1}{3N_A\sigma}\sqrt{\frac{3RT}{M}}C_{mol} \tag{3.24}$$

Where C_{mol} is the molar heat capacity, which is constant for an ideal gas. At the viscous flow the thermal conductivity for an ideal gas is pressure independent, which is important for estimating the thermal conductance of a GGHS. The relation from Eq.3.24 also explains why the lighter molecules have higher thermal conductivity, for it decreases as the molar mass increases and it is also proportional to $\sqrt{T}$, Fig.3.3 illustrates the thermal conductivity for several gases as a function of temperature.

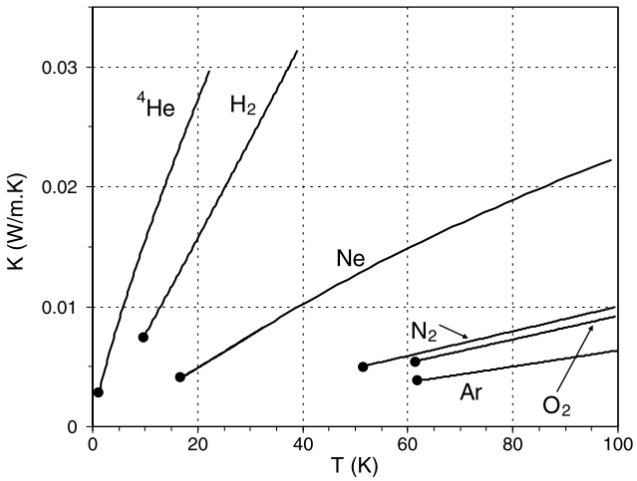

Figure 3.3: Low temperature thermal conductivity of some selected gases [7].

Being the cross section not easily obtained, an alternative to estimate the free mean path is possible to obtain. With the same deduction used to obtain the thermal conductivity k it is possibly to obtain the viscosity, which happens to be proportional to k. These viscosity values are tabulated for the most type of gases. Expressing the free mean path in function of viscosity, comes [8]:

$$\lambda = 3.62\frac{\eta(T)}{P}\sqrt{\frac{T}{M}} \quad \text{(SI)} \tag{3.25}$$

Where, $\eta(T)$ is the viscosity. Known the free mean path, it is possibly to determine the type of gas flow. As explained before, when the free mean path is much smaller than the length (i.e the gas gap) of the system ($\lambda \ll \delta$) the gas flow is viscous and at this regime the thermal conductance will be pressure independent, Eq.3.24. This regime also corresponds to the ON state of the GGHS, this is an important result because it allows to quantify the thermal conductivity of different gases, as shown in Fig.3.3.

3.2.2 Molecular flow

The molecular flow is achieved when the free mean path is higher than the gap ($\lambda \gg \delta$). At this regime the conduction is poor, which is desired in the OFF state, since the gas particles have a long free mean path and they will mainly collide with the walls, .

The heat flow rate, as seen before in Eq.3.17, is proportional to the geometry of the body and to the k obtained at Eq.3.15,

$$\dot{Q} = \frac{1}{3} C \, \overline{v} \, \lambda \frac{S}{L} \Delta T \tag{3.26}$$

The heat capacity C is proportional to the ideal gas constant R, to the number of molecule's degrees of freedom f and to the particle density n ($n = N/V$).

$$C = n \frac{f}{2} R = \frac{N}{V} \frac{f}{2} R \tag{3.27}$$

The equation of state of a hypothetical ideal gas is $PV = Nk_BT$. Remind $R = N_A k_B$, considering the ideal gas equation and the previous relation, the heat capacity is,

$$C = N_A \frac{f}{2} \frac{P}{T} \tag{3.28}$$

Since a simple approximation of the heat flow rate at the molecular flow is desired, it is considered that the mean free path is almost equal to the length of the system ($\lambda \approx L$). From Eq.3.23 the velocity is proportional to $\sqrt{T/M}$. So, the heat flow rate from Eq.3.26 becomes proportional to:

$$\dot{Q} \propto \frac{P}{T} \sqrt{\frac{T}{M}} \, L \, \frac{S}{L} \, \Delta T \; = \; \frac{P}{\sqrt{TM}} \, S \Delta T \tag{3.29}$$

From this relation we obtain the heat flow rate in the molecular regime is pressure dependent and it doesn't depend on the length of system (gap length independent). If a low $\dot{Q}$ is desired in a switch, it is necessary to achieve a low pressure between the cold and hot walls. The molecular heat flow rate from the kinetic theory of gases is [9]:

$$\dot{Q} = \alpha S \left(\frac{\gamma + 1}{\gamma - 1} \right) \sqrt{\frac{R}{8\pi MT}} \, P \Delta T \tag{3.30}$$

where α is the accommodation coefficient and γ the heat capacity ratio ($\gamma = c_P/c_V$). Remember that in this regime the gas molecules basically strikes with the surfaces. When a gas molecule with a temperature T_1 comes from the hot surface it strikes the cold surface with temperature T_2 ($T_1 > T_2$), giving up some of its energy when collide. However, the gas molecule remains at somewhat higher temperature T_2' than the cold wall, this occurring because it does not maintain physical contact long enough to establish thermal equilibrium with the surface. This effect is expressed through the accommodation coefficient α, Tab.3.1.

Temperature(K)	Helium	Nitrogen	Air
300	0.29	0.29	0.8-0.9
77	0.42	0.53	1.0
20	0.59	0.97	1

Table 3.1: Accommodation Coefficients for Several Gases at Three Temperatures. From *Cryogenic Process Engineering* [9].

3.2.3 Combined (or intermediate) flow

This regime corresponds to the transition between the viscous and molecular flow and it has both contributions, being more complex to obtain a model. Meanwhile the next equation describes somehow this mixed flow:

$$\frac{1}{K_{\text{eff}}} = \frac{1}{K_m} + \frac{1}{K_v} \tag{3.31}$$

Such equation was empirically proposed by *Tantos* [10], considering small temperature differences of a monoatomic gas and a large radius ratio of the coaxial cylinders. A very good agreement between Eq.3.31 and experimental data on a GGHS was reported in [11].

As explained before, an important characteristic of a GGHS is its thermal conductance K (W/K), this is $\dot{Q}/\Delta T$ for small ΔT. An ON state requires a high thermal conductance, corresponding to the viscous regime and the OFF state aims to low thermal conductance, corresponding to the molecular regime. Both types of flow are represented in Fig.3.4.

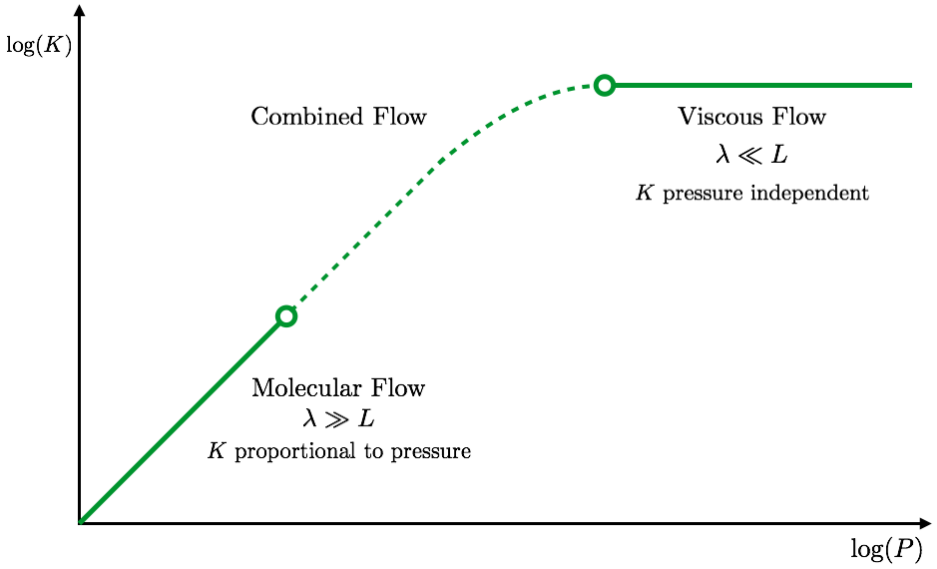

Figure 3.4: Thermal conductance between two parallel surfaces as function of pressure.

3.3 Thermal conductivity in solids

The heat transfer in a solid is due to lattice vibrations (phonons) and to conduction electrons. In pure metals, nearly all heat is carried by the electrons. In impure metals, alloys and semiconductors, an appreciable proportion of the thermal conductivity is due to lattice conduction. In dielectric crystals and amorphous insulating solids, as expected, all the heat is transported by the phonons.

These carriers of heat do not move ballistically from the hotter part of the material to the colder one. They are scattered by other electrons, phonons, defects of the lattice and impurities. The result is a diffusive process which can be described as a gas diffusing through the material (Eq.3.15).

The main scattering processes are phonon–phonon, phonon defect, electron impurity, electron–phonon, or point defects and more rare electron–electron. The thermal resistivity due to the various scattering processes are additive. For the phonons[12],

$$\frac{1}{k_{ph}} = R_{pp} + R_{pe} + R_{pi} \tag{3.32}$$

where R_{pp} is caused by phonon-phonon scattering, R_{pe} by phonon-electron (present only in metals and electrical conductors), R_{pi} by scattering from impurities or point defects.

In the case of metals and electrical conductors, for the electrons, the thermal resistivity is,

$$\frac{1}{k_e} = R_{ei} + R_{ep} \tag{3.33}$$

where R_{ei} is caused by impurity scattering and R_{ep} by scattering from phonons. Since the number of phonons increases with increasing temperature, the electron–phonon and phonon–phonon scattering processes are temperature dependent. The number of defects is temperature independent and correspondingly, the mean free path for phonon defect and electron defect scattering does not depend on temperature. The global thermal conductivity corresponds to the sum of both heat carriers, k_{ph} and k_e.

3.3.1 Lattice Conductivity

For phonons at temperatures well below the Debye's[2] temperature ($T \ll \theta_D$) the number of phonons is rather small, consequently the phonon-phonon scattering processes are rare and the phonons which carry the heat are scattered by crystal defects. At this regime the specific heat is proportional to T^3 [14], being the thermal conductivity at this regime proportional to:

$$k_{ph} \propto C_{ph} \propto T^3 \tag{3.34}$$

[2]The Debye temperature is the temperature of a crystal's highest normal mode of vibration, i.e., the highest temperature that can be achieved due to a single normal vibration[13].

With increasing temperature the phonon-phonon scattering process becomes dominant, since the number of phonons increases with increasing temperature. As consequence the proportion T^3 vanishes and the heat capacity tends to stabilize for high temperatures ($C = 3R$) and so does the heat conductivity.

3.3.2 Electronic Thermal Conductivity

Usually in a metal, the electronic contribution is much larger than the lattice contribution due to the strong difference in the velocity of heat carriers. Again there are two phenomena which produce the scattering of the electrons as heat carriers:

- The lattice may be distorted because of several reasons as vacancies and impurities. These lattice defects cause the the so-called impurity scattering, R_{ei}. At low temperatures, this thermal resistance is the constant electronic thermal residual resistance typical of metals.

- The other contribution is due to phonons, R_{ep}.

At low temperatures the number of phonons is small and the scattering of electrons from lattice defects and impurities dominates. We obtain a temperature-independent electronic mean free path resulting in the following equation for the electronic thermal conductivity:

$$k_e \propto C_e \propto T. \tag{3.35}$$

At high temperatures, the thermally excited phonons are the limiting scatterers for the heat conducting electrons. Because the number of thermally excited phonons increases with temperature, we find for the electronic thermal conductivity in the electron–phonon scattering region a thermal conductivity which decreases with increasing temperature. Despite the linear increasing of the heat capacity with temperature, the number of collisions with phonons also increases, resulting in a reduction of the thermal conductivity with temperature.

Again, there are two scattering processes dominating in different temperature regions and with opposite temperature dependencies. As a result, the electronic contribution to the thermal conductivity also goes through a maximum, as observed at Fig.3.5.

The value and position of this maximum strongly depends on the perfection of the metal. With increasing impurity concentration, the maximum is diminished and shifted to higher temperature (e.g copper in dashed lines in Fig.3.5). In a disordered alloy the scattering of electrons and phonons becomes comparable, no observable maximum (eg. aluminium alloy).

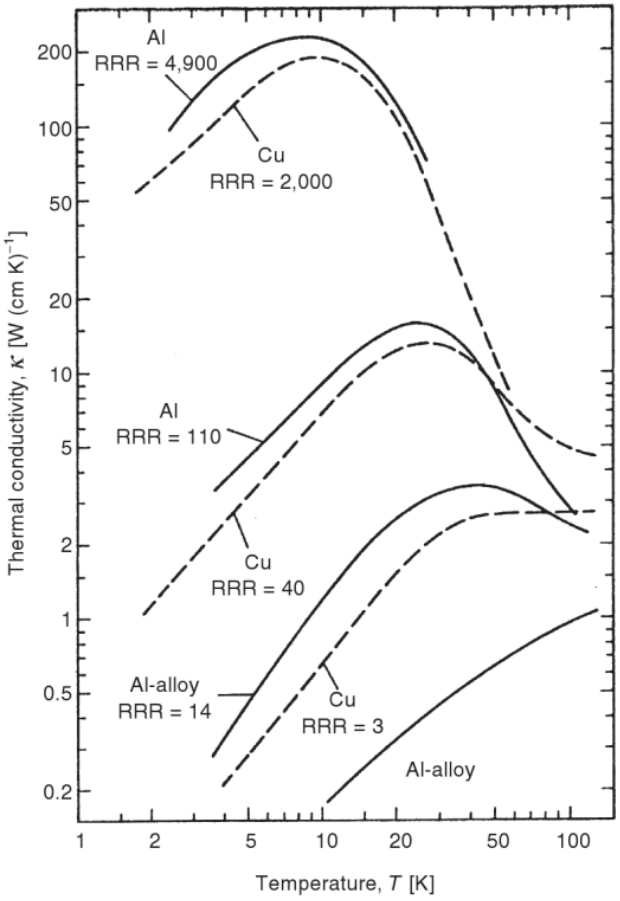

Figure 3.5: Temperature dependence of the thermal conductivities of Al and Cu of varying purity (expressed as their residual resistivity ratio) [15].

The residual-resistivity ratio (RRR) describes the purity of a metal, it is the ratio of the resistivity of a material at room temperature and at 0 K.

$$RRR = \frac{\rho_{300K}}{\rho_{0K}} \tag{3.36}$$

A perfect metal is free of scattering mechanisms so would expect $\rho_{0K} = 0$, which would cause RRR to diverge. However, this doesn't occur because the defects such as impurities or grain boundaries act as scattering sources at low temperatures, contributing to a temperature independent ρ_{0K} value.

The knowledge of such materials properties is important when designing a heat switch. A good thermal conductor (e.g copper) is desired for the construction of the blocks so it does not jeopardize the gaseous conductance in the gap at the high thermal conductance state (ON). For the low thermal conductance state a low thermal conductor is desired (e.g stainless steel) for the manufacture of the supporting shell, which remains as the only conduction path once the gas is removed from the gap.

CHAPTER 4

GGHS PROTOTYPE

This chapter describes all thermal and mechanical requirements to build the gas-gap heat switch. Considering all requirements a solution was adopted. An analytical approach was made, optimizing the geometry for an ON/OFF thermal conductance. The heat switch was designed with a CAD software (*SolidWorks*^{TM}).

4.1 Thermal requirements and adopted solution

As said before at Chapter 2.3 the Inter University Accelerator Centre (New Delhi) is implementing a cryogen-free apparatus for measuring magnetic properties. A 6 T superconductor magnet is used and a particular cryocooler acts as a cold source (SRDK 415D), the cooling power as function of temperature is known from the manufacturer data-sheet (1.5 W @ 4.2 K, see Annex 8.2). The parasitic heat loads were estimated, so the remaining cooling power could be diverted to the variable temperature insert (VTI).

The estimation of available power is a necessary parameter to develop a gas gap heat switch.

The cryocooler of the IUAC's lab has a total cooling power of 1.5 W at 4 K. Considering all safety factors, the power needed to keep the superconductor coil working is about 1W, remaining about 500 mW to be diverted to the VTI.

A gas gap heat switch (GGHS) will be thermally connected between the cold finger and the VTI, allowing to close or open this thermal connection. The principal advantage of this configuration is the possibility to open the VTI without warming up the coil. When opening the VTI to the room temperature the heat switch must stay at OFF state. Because at this state the power diverted from the cryocooler will be relatively low, at maximum 0.5 W. With this requirement it is possibly to define the switch's geometry.

The prototype built has a classical geometry, as schematized in Figs.4.1 and 4.2. It consists in a copper cylinder coaxial to a copper tube-like separated by a 100 μm gap, this

gap width was chosen to prevent mechanical complications.

A 100 μm thin stainless steel supporting shell (SSSS) was chosen to surround the cold copper block, assuring the sealing and centering the two copper blocks. This thickness is also a compromise to insure the mechanical rigidity of this assembly and to obtain a relatively high thermal isolation between the switch ends in the OFF state.

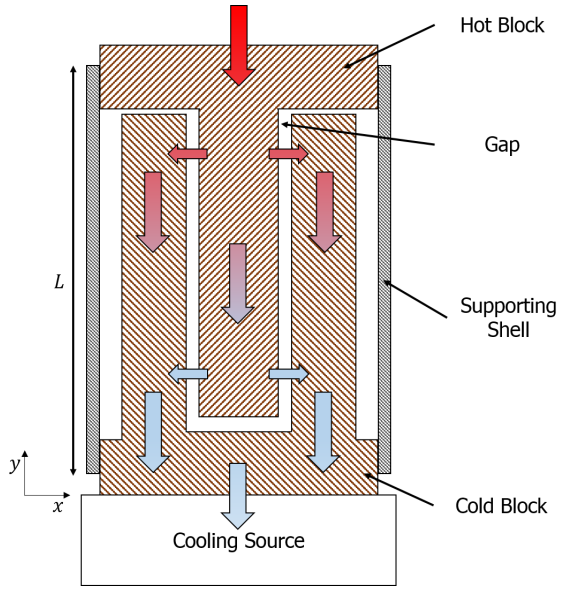

Figure 4.1: General scheme of a gas-gap heat switch. The arrows indicate the heat path directions used to calculate the thermal resistances.

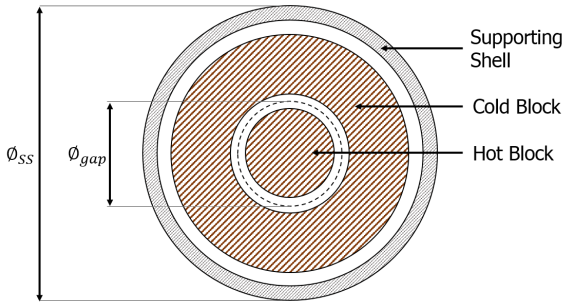

Figure 4.2: Cutaway of a gas-gap heat switch.

From the discussion hold in Chapter 3 the thermal resistance R_{gap} (in K/W) is proportional to the pressure in the OFF state, the pressure inside the gap being sufficiently low to assure that R_{gap} becomes negligible, being the stainless steel tube the only thermal conductor at this state. A thermal model used to assist the determination of the thermal conductance is schematized in Fig.4.3, where the pressure dependent gas-gap thermal resistance is drawn as a variable resistor.

With this model, it is possibly to choose a geometry for the stainless steel shell (radius and length). The geometry is defined upon the worst case scenario which is having one side at 300 K and the other at 4 K (i.e. the maximum temperature difference).

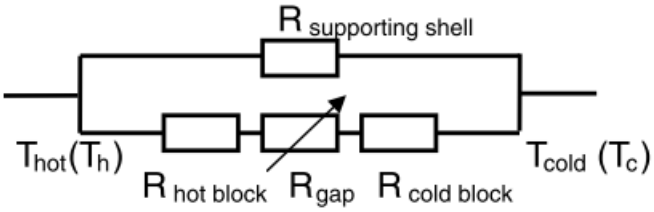

Figure 4.3: Heat conduction elements considered in the thermal model between hot and cold blocks of a gas-gap heat switch [7].

The power through the shell is calculated with Eq.3.20. The values for the stainless steel thermal conductivity are found at NIST-Cryogenics Material Properties [16].

To select the best geometry (outer diameter and length) once the thickness fixed, thermal power was calculated as a function of the outer diameter for various lengths, as represented in Fig.4.4. Since a good ON state is also desired, the ratio of the gap section (S=$\pi\, L\, \varnothing_{\text{gap}}$) and length (100 μm gap) was calculated, Fig.4.5. This will give an estimation of the conduction optimization for the ON state.

In the OFF state the heat flow direction is along the shell (y direction) and at the ON state is through the gap (x direction), check arrows at Fig.4.1. The heat path direction is important to calculate the section to length ratio for both states.

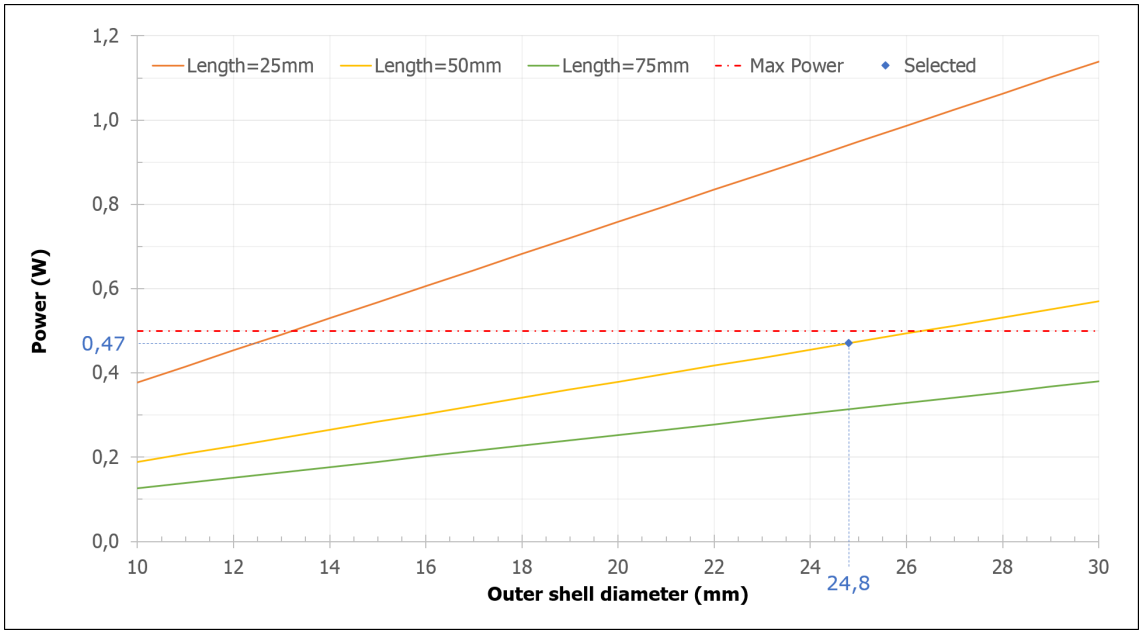

Figure 4.4: Power (in W) through SS304L between $T_{\text{c}} = 4$ K and $T_{\text{h}} = 300$ K as a function of outer shell diameter $\varnothing_{SS}$ (in mm) for various lengths (in mm), tube thickness = 100 μm.

As can be inferred from Fig.4.4 the $\dot{Q} < 0.5$ W at extreme ΔT is only possible for the smaller $\varnothing_{SS}$ and/or longer L. Stating $L = 50$ mm as a reasonable length (both from manufacture point of view and from fitting in IUAC's setup) turns $\varnothing_{SS} < 26$ mm.

The case of a 75 mm length, despite of always checking the power limit for that range of diameters, a long shell lead to a low rigidity tube resulting in a complicated manufacture. Also, it couldn't fit on the IUAC's setup.

The selected geometry is at 50 mm length curve with 0.47 W, 24.8 mm for the outer diameter and S/L ratio $= 26$. This configuration lead to less mechanical problems and with reasonable dimensions. On a private communication with the workshop manufacturer this geometry seems reasonably. However the workshopping would bring some uncertainty in the thickness of the stainless steel tube, at maximum it could reach 130 μm, so the ordered length was 60 mm to forearm this uncertainty.

From the scheme of Fig.4.1 some of the available length of the tube is thermalized at hot and cold blocks considered each as isothermal. Then, some part of this length does not contribute in the conduction, it was defined the effective length is 54 mm (thermal power at extreme $\Delta T = 0.44$ W).

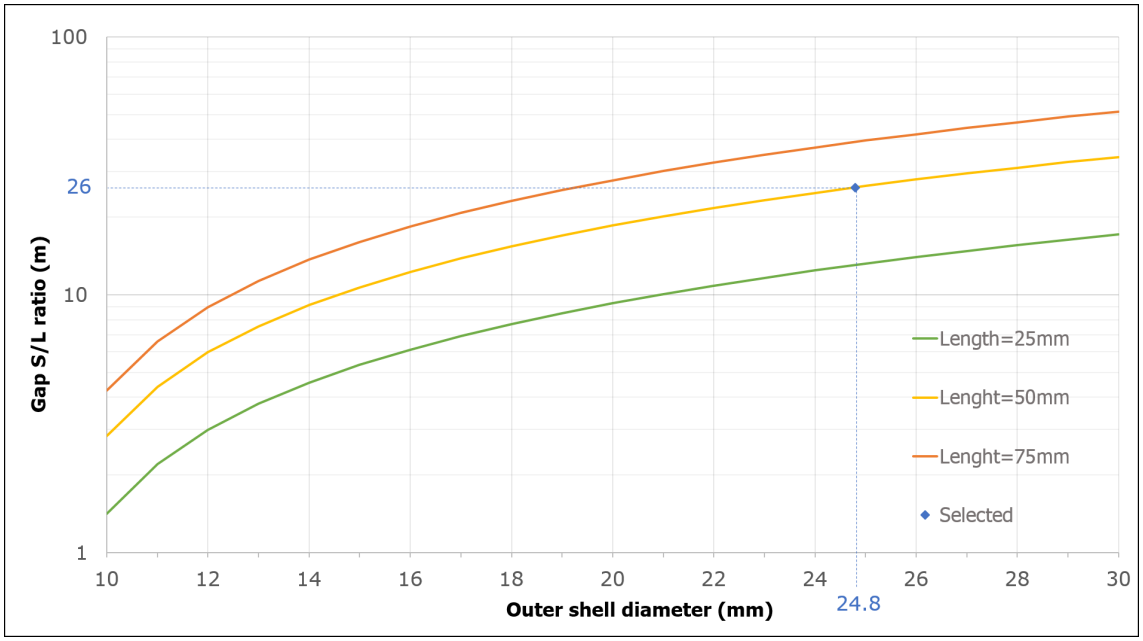

Figure 4.5: Gap S/L ratio for SS304L as a function of outer shell diameter $\varnothing_{SS}$ (in mm) for various lengths (in mm).

4.2 Mechanical requirements and adopted solution

The heat switch consists of two coaxial copper blocks. It was designed to be assembled in a ∅68 mm flange (as imposed by the diameter of the cryocooler cold finger). The copper blocks were built to guarantee a gap of 100 μm. The cold and hot blocks were machined from a cylinder with ∅68 and ∅42 mm, respectively.

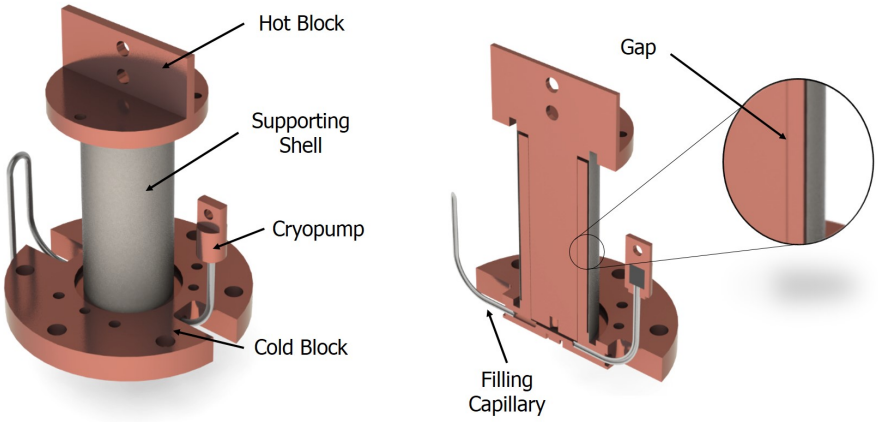

Figure 4.6: Gas-gap heat switch designed in *SolidWorks*^{TM}.

The centering of both blocks, the switch sealing and mechanical rigidity are assured by a 100 μm thickness wall supporting shell with a outer diameter $\varnothing_{out} = 24.8$ mm and a 60 mm length made in stainless steel

To control the gas pressure inside the gap a cryopump was designed and coupled to the cold block (Section 4.4) through a stainless steel capillary, Fig.4.6.

The heat switch is filled through the filling capillary at the cold block. The cold block has two holes that makes connection from outside, one hole for the cryopump and other for the filling capillary, Fig.4.6.

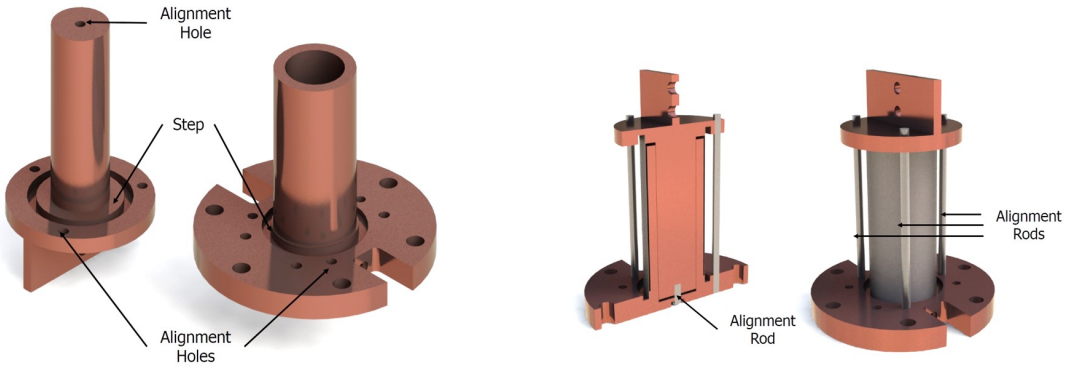

Figure 4.7: Gas-gap heat switch designed in *SolidWorks*^{TM}. From left to right: cold block, hot block and detailed view of alignment rods.

To guarantee the concentricity of both blocks, the shell fits in a 3 mm step, see Fig.4.7. Also, around this step there is a small pit to assist the deposition of the solder.

To prevent a possible misalignment, which could lead to thermal short-circuit, it was used four alignment rods to maintain the correct position during the soft soldering process, see Fig.4.7.

The alignments rods are removed after soft soldering. Removing the central rod will leave a hole at the cold block: a copper stopper fits the hole, allowing the sealing of the switch, see Fig.4.8.

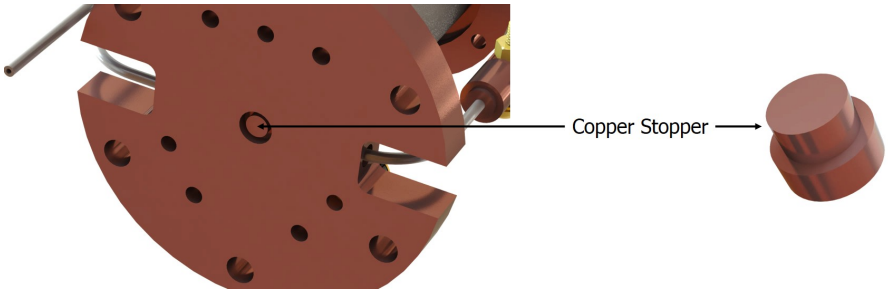

Figure 4.8: Gas-gap heat switch designed in *SolidWorks*™. Detailed view of the stopper.

More detailed info about the dimensions are found in the technical drawings at Appendix 9.1.

4.3 Thermal conductance - analytical approach

4.3.1 OFF state

As said before, the OFF state is assured if the pressure inside the switch is sufficiently low to assume that the only material conducting heat is the stainless steel shell.

The chosen shell has a $\varnothing_{out} = 24.8$ mm, $\varnothing_{in} = 24.6$ mm and 54 mm effective length. The thermal power through the shell is given by Eq.3.20, rewritten as:

$$\dot{Q}_{SS} = \frac{\pi(\varnothing_{out}^2 - \varnothing_{in}^2)}{4L} \int_{T_c}^{T_h} k_{SS}(T)\, dT \tag{4.1}$$

Fig.4.9 expresses the power versus ΔT in such a cylinder, the cold side being at 4 K. The values for the thermal conductivity integral were calculated iteratively in Microsoft Excel Visual Basic Program® from $k(T)$ values from [16] with the trapezoidal rule:

$$\int_{T_c}^{T_h} k_{SS}(T)\, dT \approx (T_h - T_c)\, \frac{k_{SS}(T_c) + k_{SS}(T_h)}{2} \tag{4.2}$$

For low temperatures ($\Delta T \leqslant 6$), the thermal resistance in the OFF state is 11 K/mW (0.09 mW/K). With this configuration we obtain 436 mW for the worst case ($4 - 300$ K).

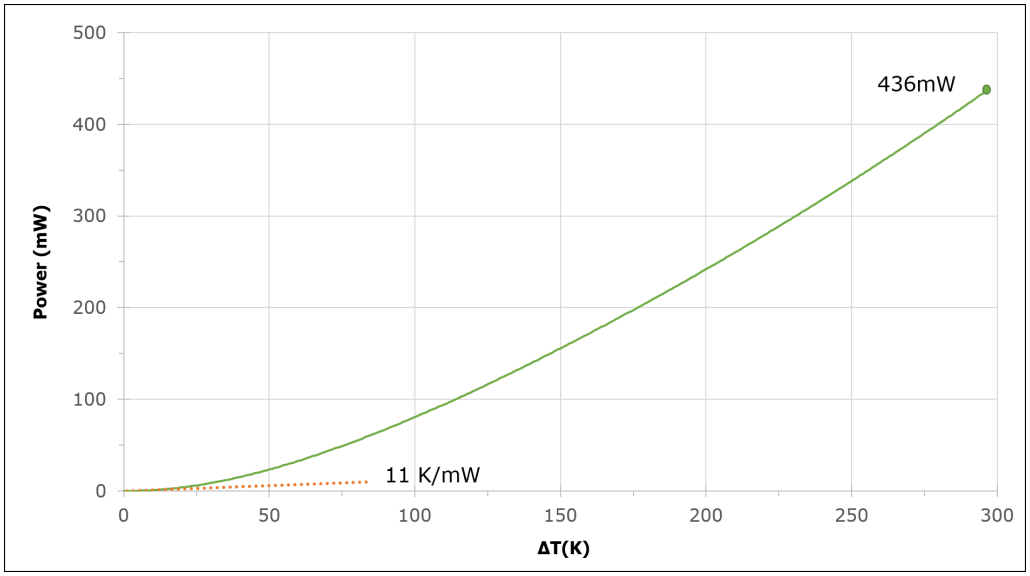

Figure 4.9: Analytic curve of the power $\dot{Q}$ through the supporting shell of the switch versus $\Delta T = T_{\text{hot}} - T_{\text{cold}}$, $T_c = 4\ K$.

4.3.2 ON state

In the ON state the heat conduction is done by the gas, copper and shell, in an association as seen in Fig.4.3. Meanwhile the shell thermal conductance is negligible when comparing to the gas ($K_{SS} \ll 1\% K_{\text{gas}}$), so it is ignored on the calculations. The global thermal resistance in the ON state is:

$$\frac{1}{K} = \frac{1}{K_{\text{gas}}} + \frac{1}{K_{\text{Cu}_h}} + \frac{1}{K_{\text{Cu}_c}} \tag{4.3}$$

Meanwhile, the previous equation is valid if the heat flux flow is constant through one direction. Given the switch's geometry it is not trivial to make a series or parallel association between the gas and copper blocks, because the heat flow on the copper blocks varies along the copper length. It can be shown that the effective length to be considered is half the geometrical length as long as the copper thermal resistances are close (i.e. leading to an uniform heat flux in the gas) [7, 11] and hence use the association as seen in Fig.4.3.

The global thermal conductance was calculated for several temperature differences ΔT[1] in Microsoft Excel®. The mean temperature T_M was considered for the determination of thermal conductivity of the gas and copper, this approximation is valid in the considered intervals. Considering Eqs.3.17 and 4.3 the heat flux for this state comes:

$$\dot{Q}_{\text{ON}} = \left(\frac{1}{K_{\text{gas}}} + \frac{2}{K_{\text{Cu}}} \right)^{-1} \Delta T \tag{4.4}$$

In Eq.4.4, $K_{\text{Cu}_h} \approx K_{\text{Cu}_c} = K_{\text{Cu}}$.

[1] $\Delta T = T_{\text{hot}} - T_{\text{cold}}$ with $T_{\text{cold}} = 4\text{K}$

Also remind that, the thermal conductance K is proportional to the thermal conductivity k and the S/L ratio. For the gas, in SI units, the S/L ratio is 30.43 (considering a gap of 100 μm) and for the copper is 7×10^{-3} (considering its half length).

It was selected the Helium-4 because of the temperature range applied (minimum temperature: 4 K), see Fig.3.3. The values for the copper $RRR = 50$ thermal conductivity are found at [16] and for helium gas at REFPROP [17].

If $K_{Cu} \gg K_{gas}$ the heat flux in the ON state depends only on the gas thermal conductance, because the term K_{Cu}^{-1} tends to zero, as can be verified in Eq.4.4. The curves from Fig.4.10 describes the effect of the copper on the global thermal conductance.

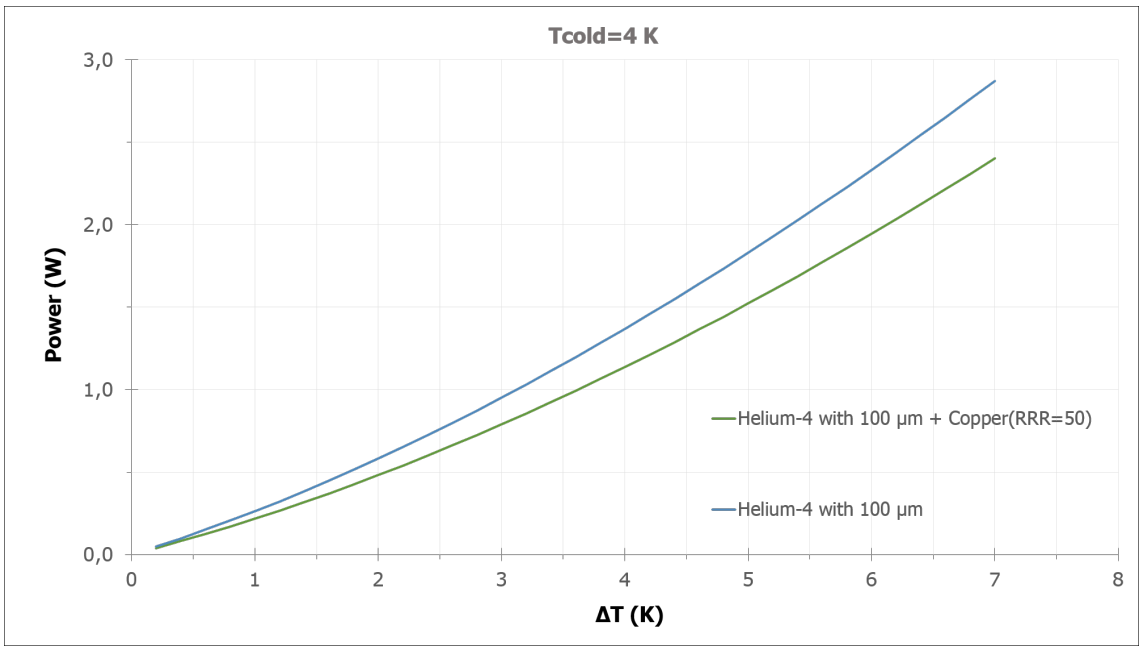

Figure 4.10: Analytic curve of the power $\dot{Q}$ through the switch versus $\Delta T = T_{hot} - T_{cold}$ in the ON state, $T_c = 4$ K.

On a first approximation the thermal conductance in the ON state is 269 mW/K for the copper curve. A better quality copper, i.e. higher purity, would improve the conduction in the ON state, approximating to the helium curve.

4.4 Cryo-pump adaptation

The amount of gas in the gap of a heat switch can be managed by using the sorption properties of an activated charcoal and benefit from a compact and small closed system. This way the actuation of the heat switch is made upon the heating/cooling of a cryopump. The heating of the cryopump is made with a 1.2 kΩ heater resistor and its cooling with the stainless steel capillary thermally coupled to the cold block.

When the cryopump cools down, the thermal energy ($k_B T$) is low (virtually no thermal agitation) and the molecules prefer to stay at the activated charcoal surfaces by Van der Walls forces. An activated charcoal can adsorb great quantities of gas (having an inner surface of 3000 $m^2 g^{-1}$).

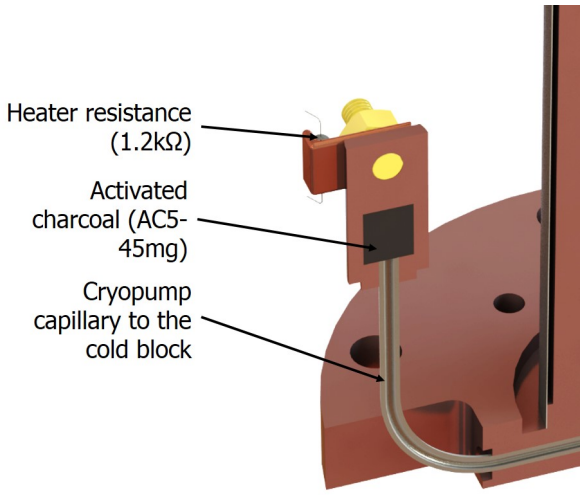

Figure 4.11: Cryopump detailed view.

In the OFF state, the power through the gas must be negligible when compared to the power through the shell, this corresponds to molecular flow, which occurs when the mean free path is higher than the length of the gap ($\lambda \gg \delta$). The power through the gas is described with Eq.3.30, it was defined that the OFF state is obtained when the gas thermal conductance is 10 times smaller than the shell ($K_{gas} \leqslant K_{SSSS}/10$). It was obtained a pressure $P_{OFF}^{MAX} = 5.3 \times 10^{-6}$ mbar at 4 K.

On the other hand, the ON state is achieved when there is sufficient pressure inside the gap to obtain a viscous flow between both blocks ($\lambda \ll \delta$). As said before, the mean free path is given by Eq.3.25. It was defined that to achieve this state the mean free path has to be at least 100 times smaller than the dimension of the gap ($\lambda \leqslant \delta/100$) [7]. It is possible to obtain the minimum pressure P_{ON}^{MIN} for Helium-4 to achieve the on state for various gas temperatures, Fig.4.12.

Given the ON and OFF pressures and considering the ideal gas law, the switch must be filled up with at least $P_{charge} = 98$ mbar at room temperature to obtain $P_{ON}^{MIN} = 1.3$ mbar

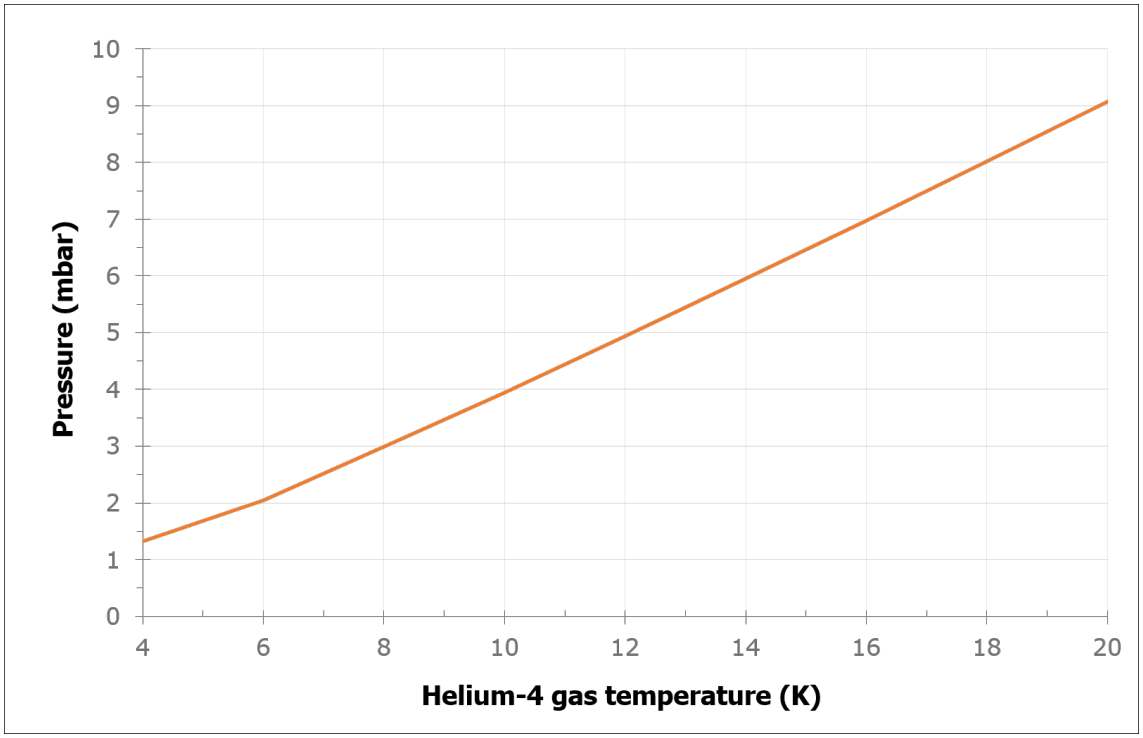

Figure 4.12: Minimum pressures P_{ON}^{MIN}, for Helium-4, to obtain the ON state for various gas temperatures with a 100μm gap.

at 4 K. However the cryopump must be capable to adsorb a amount of gas to obtain 5.3×10^{-6}mbar at 4 K to achieve the OFF state. The amount of adsorbed gas n_{ads} is:

$$n_{ads} = \left(\frac{P_{charge}}{T_{amb}} - \frac{P_{OFF}^{MAX}}{T_{cold}} \right) \frac{V}{R} \tag{4.5}$$

Where P_{charge} is the charge pressure at room temperature T_{amb}, P_{OFF}^{MAX} maximum pressure to obtain the OFF state at T_{cold}, V the volume of the switch (including the feeding mechanism) and R is the ideal gas constant.

Given the charge pressure and cryopump temperature, the amount of adsorbed gas by the carbon in grams of helium per gram of carbon can be obtained by resorting to the experimentally obtained PTQ[2] equation of state[18].

A previous cryopump was reused filled with 45 mg of the type "C" activated charcoal [18]. Known the type of coal, the amount of adsorbing need and selected gas, one can conclude that with this amount of charcoal it is possible to achieve the OFF state, i.e., the estimated off pressure.

With Eq.3.31 it is possible to calculate the "S" shaped curve, this curve showing the transient conduction regime between ON and OFF states. The estimated values for P_{OFF}^{MAX} and P_{ON}^{MIN} are shown in Fig.4.13.

[2]Three state variables: Pressure (P), temperature (T), and amount of adsorbed gas per amount of adsorbent (Q)

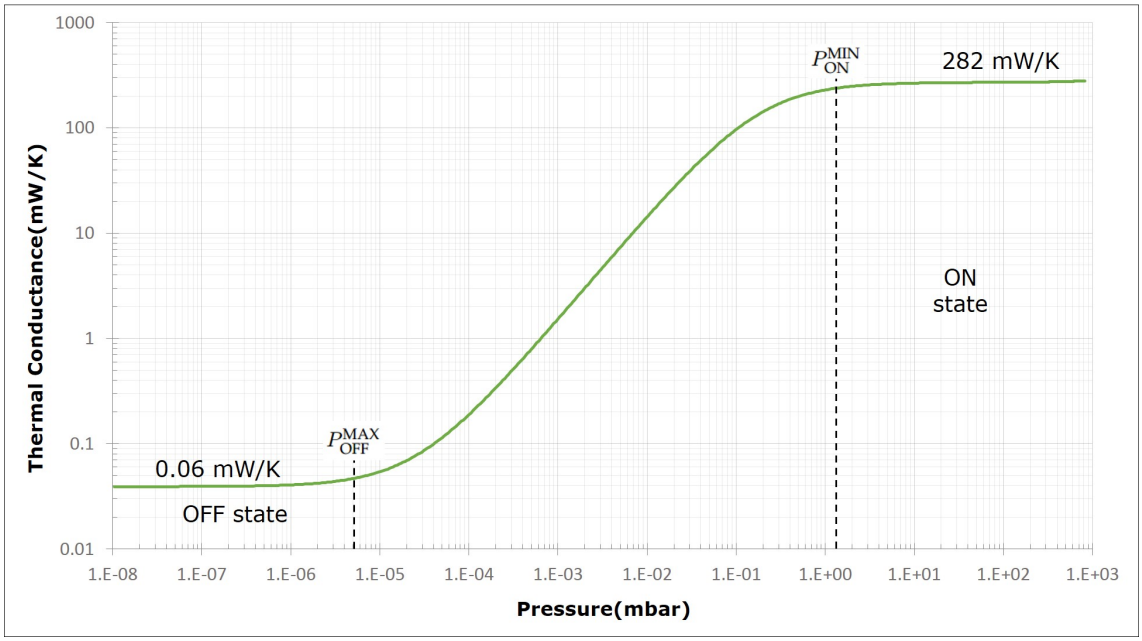

Figure 4.13: Calculated thermal conductance of the heat switch at 4 K as a function of the pressure.

It is common to represent the heat switch performance by its ON/OFF conductance ratio, this one would be 4700 at 4K.

Remind this curve is representative only for 4 K, the limit values (ON and OFF thermal conductance) vary because the thermal conductivity depends on temperature (e.g Fig.4.14).

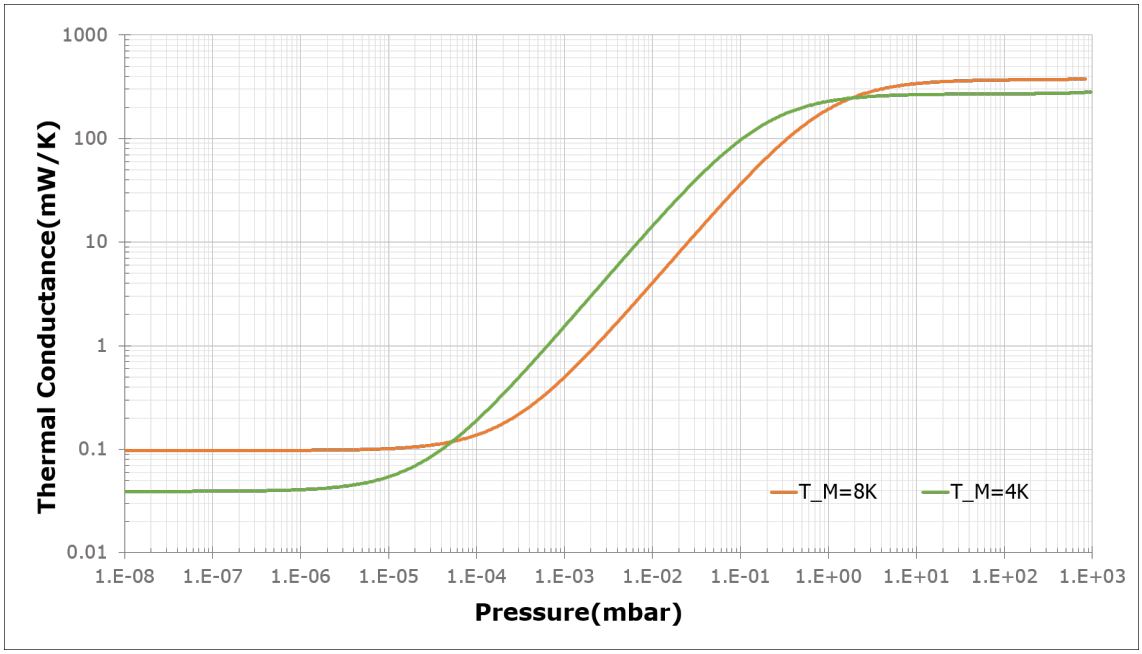

Figure 4.14: Calculated mean thermal conductance variation of the heat switch for $T_M = 4$ K and 8 K versus pressure.

Another important parameter is the cooling time and necessary power to heat up the cryopump: on heating is intended to isolate the cryopump from the cold source, this way it would not be necessary to apply too much power to heat it up. In this case it would be convenient to use a long stainless steel capillary.
As for the cooling, since the cold block is the cooling source of the cryopump, the thermal decoupling can not be too high, otherwise would take too long to cool down. It can be defined a characteristic time of thermalization ($\tau_c = R_{SS}\, C$) where R_{SS} is the thermal resistance of the stainless steel capillary which connects the cryopump to cold block and C the heat capacity of the whole cryopump, Fig.4.11.

It can be concluded that an excessive length for the connection cryopump-cold block could largely enlarge the time of cooling. It was selected a capillary with diameters 1.5×2 mm and 30 mm length. For which only 1 mW is necessary for reaching 25 K and about one hour to cool down from 25 to 4 K ($\tau_c \approx 70$ s).

CHAPTER 5

EXPERIMENTAL SETUP

This chapter describes the mechanical assembly of the device including its assembly on the cryocooler used for testing. The control and data acquisition is also briefly described.

5.1 Mechanical assembly

The construction of this switch requires high stringency due to the reduced dimensions of both the gap (100 μm) and the thin stainless steel shell (100 μm). The pieces were manufactured in a precision metalwork at *A. M. Tita, Lda* located at Santa Marta de Corroios. The copper blocks were built in a lathe machine and the shell by electro-erosion. All tolerances were respected, otherwise it would be impossible to obtain a 100 μm gap between the copper blocks.

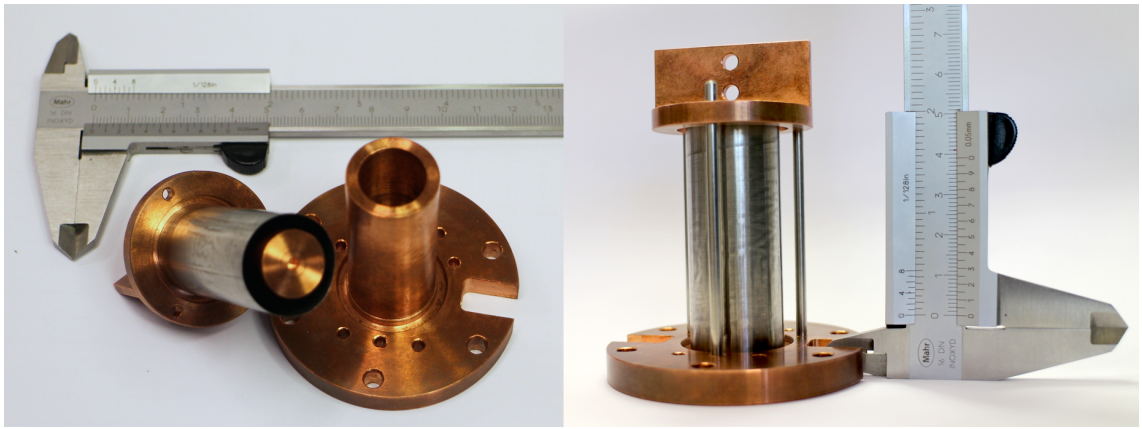

Figure 5.1: Photo of the two copper blocks and the stainless shell tube. At right, pieces mounted with alignment rods.

Four stainless steel rods were projected and used to assist the alignment and concentricity of both blocks while assembling, as seen in Figs.5.1 and 5.2.

The shell is jointed to both copper blocks and the capillaries to the cold block. To assure a good brazed joint, the surfaces were polished and cleaned in a ultrasound bath before soft soldering, see Fig.5.2.

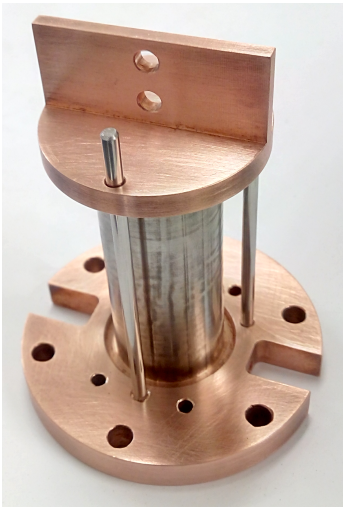

Figure 5.2: Copper blocks after polish.

The shell was jointed to the copper blocks with a soft solder, $Sn_{96.5\%}Ag_{3.5\%}$ melting point of 221°C, assisted with a liquid flux[1].

The switch was heated up to approximately 220°C in a 600 W home-made heating aluminium plate, see Fig.5.3. After reaching the melting point, the surface to be brazed was wetted with liquid flux and then the filler metal was added. The first solder ring was made in the heavier block (cold block mass: 314 g). After cooling, the switch was flipped and the process was repeated on the other block (hot block mass: 188 g), the previous solder ring not being affected. The liquid flux can be very corrosive and could damage the thin shell, therefore the switch was cleaned up again in a ultrasound bath.

The switch was then heated up to approximately 190°C for soldering the filling capillaries. It was used a flux-cored soft solder $Sn_{60\%}Pb_{40\%}$ with a melting point of 180°C to joint the capillaries to the cold block. A lower melting point solder was selected so it would not compromise the previous brazing.

At the end, when the switch is soldered, the alignment rods were removed. The central alignment rod goes through the hot and cold block, see Figs.4.7 and 4.8, leaving a hole at the cold block when removed. A copper stopper (see Appendix.9.1) was built at Physics department workshop and then it was soldered to the cold block with the same flux-cored soft solder used for the capillaries. Since, this was the last soldering, it was made with caution to prevent damaging the previous soldering.

[1]Solder: *Castolin* 157 and Flux: *Castolin* 157A

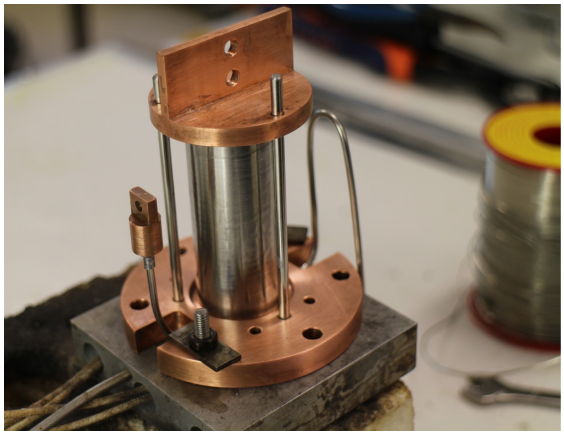

Figure 5.3: 600 W home-made heating aluminium plate.

After soldering, the surfaces were oxidated so it was necessary to clean the heat switch with nitric acid (10%). To assure a good thermal contact, the surfaces were cleaned (with acetone) and polished (steel wool), paying special attention to the surface of the cold block because this one will be directly attached to the cold finger.

5.1.1 Leak Detection

After soldering, the heat switch would be ready for testing if there are no leaks. The leakage tests were performed with two techniques: Helium-4 vacuum technique and sniffing test, the last one was used to detect the precise location of the leak. The tests were performed with a *INFICON*®(model: UL1000) helium leak detector.

There were several problems concerning the sealing of the heat switch. Initially the leakage test was performed with the vacuum technique, obtaining a leak rate of $\sim 10^{-3}$ mbar.L/s, for a good sealing it was considered the gas leak should be inferior to 2×10^{-7} mbar.L/s. It was thought the problems came from the solder ring copper-shell. So, the soldering was repeated. Nevertheless the problems persisted, obtaining $\sim 10^{-4}$ mbar.L/s, the leakage tests were performed with the sniffing test to obtain the specific location of the leaks.

It was detected several spot leaks along the thin stainless steel tube. Thus, it was considered the shell was practically permeable. The first solution was to cover the shell with VGE-7031 varnish, Fig.5.8. However this solution works temporarily (leak rate: $< 10^{-7}$ mbar.L/s) because the cycle of cooling/heating eventually causes the varnish to crack. Still, it was possible to obtain some experimental results.

When the varnish cracked, it was necessary to apply a permanent solution. That solution was to cover the shell with an epoxy resin, it was used a Stycast2850FT with a catalyst 24, see Fig.5.4, this material was selected because its thermal conductivity is approximately the same order of magnitude of the stainless steel [19] and it will be capable of masking the leaks. This solution came successful (no leaks detected), allowing to obtain results without any interferences.

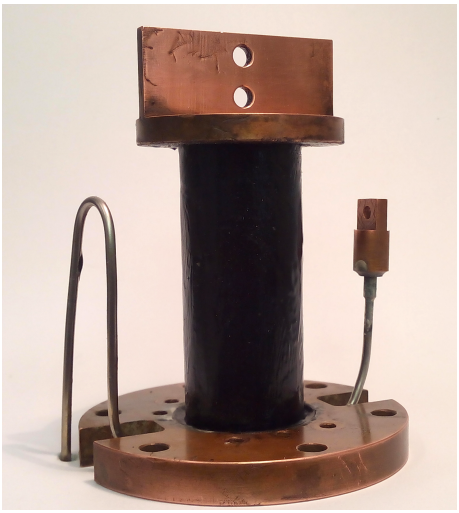

Figure 5.4: Heat switch covered with Stycast2850FT as an attempt to repair the leaks.

5.1.2 Gas feeding and manifold

The pressure inside the switch was managed by a manifold composed by needle valves (V1 & V5), ball valves (V1-4 & V6-8), vacuum manometers (M1 & M2): piezoresistive and baratron^{TM} capacitance manometers[2], 1 L calibrated volume (volume 1), 50 L helium cylinder (volume 2), rotary vane pump and two copper "coil" tubes (C1 & C2), as represented in Fig.5.5.

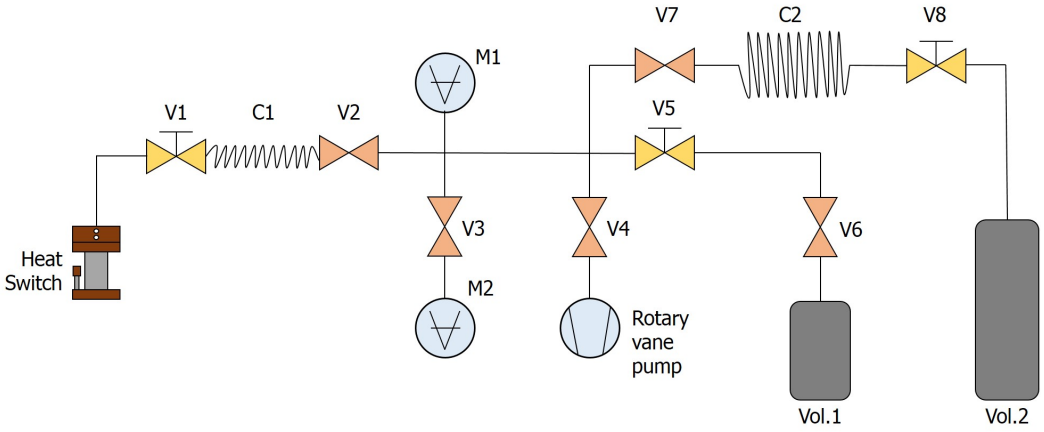

Figure 5.5: Gas feeding scheme.

To test the ON state it is necessary to fill the calibrated volume with a determined pressure and open all the valves (except V4 and V7) to the switch. Before charging, the helium gas went through the conductance C2 which was immersed in a liquid nitrogen bath to purify the gas. Also, several purges were made to obtain a clean environment. The needle valves allows to control the gas flow and to fill the volume (V6) with the desired

[2]Range:0.1-1000 mbar or 0.001-10 mbar, whenever was necessary the baratron was switched.

pressure. The conductance C1 is long enough and thin to allow a good thermal decoupling from the cold zone to the hot zone, Fig.5.6.

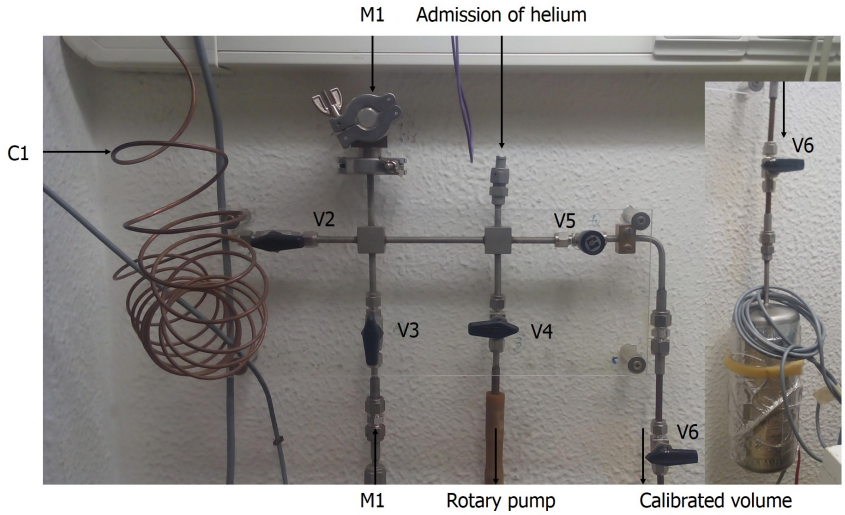

Figure 5.6: Manifold. The conductance C1 separates the cold zone from the hot.

5.2 Cryogenic assembly

A two stage cryocooler was used to test the heat switch from *SHI Cryogenics Group*, model RDK-408D2 4K, Fig.5.7 Its operation is based in a Gifford-McMahon thermodynamic cycle using compression and expansion cycles of helium.

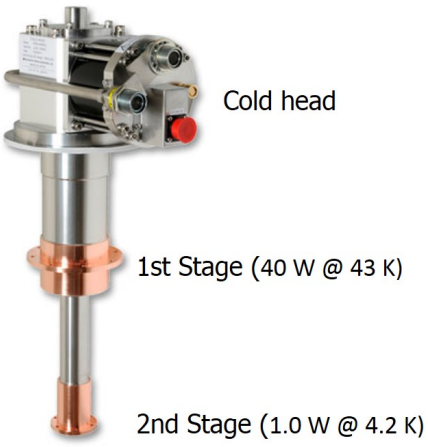

Figure 5.7: Gifford-McMahon cryocooler, model:RDK-408D2 [20].

A copper radiation shield is screwed, on the first stage, reaching a minimum temperature of 28 K. The second stage, where the heat switch is connected it has another shield, also in copper, such 2nd stage has a capacity of 1 W at 4.2 K (manufacturer datasheet at

Annex 8.2). Both stages are inside a stainless steel vacuum chamber, about 10^{-6} mbar is reached by a turbo pump and its own cryo-pumping made by the cryocooler.

The cold block of the heat switch was smeared with grease (Apiezon) and directly coupled to the cold finger along with 4 screws.

For the temperature measurements three *Cernox*^{TM} thin film resistances were used as temperature sensors. They were coupled to the cold and hot blocks and to the cryopump and measured by a *CryoCon*^{TM} temperature controller, model 34.

To control the temperature of the second stage (i.e. the cold block) a pair of heater resistors controlled in a closed loop from the temperature controller (max. power: 50 W) were used. For the cryopump a 1.2 kΩ heater resistor also controlled by another loop from the temperature controller (max. power: 25 W) was used. For the hot block a 1.2 kΩ heater resistor controlled by a *Agilent*^{TM} DC power source with a maximum power of 2 W (50 V), model E3631A, was used.

The pressure inside the switch was measured through a piezoelectric transducer with a multimeter, *Keithley*^{TM} (model 2001), see Fig.5.8.

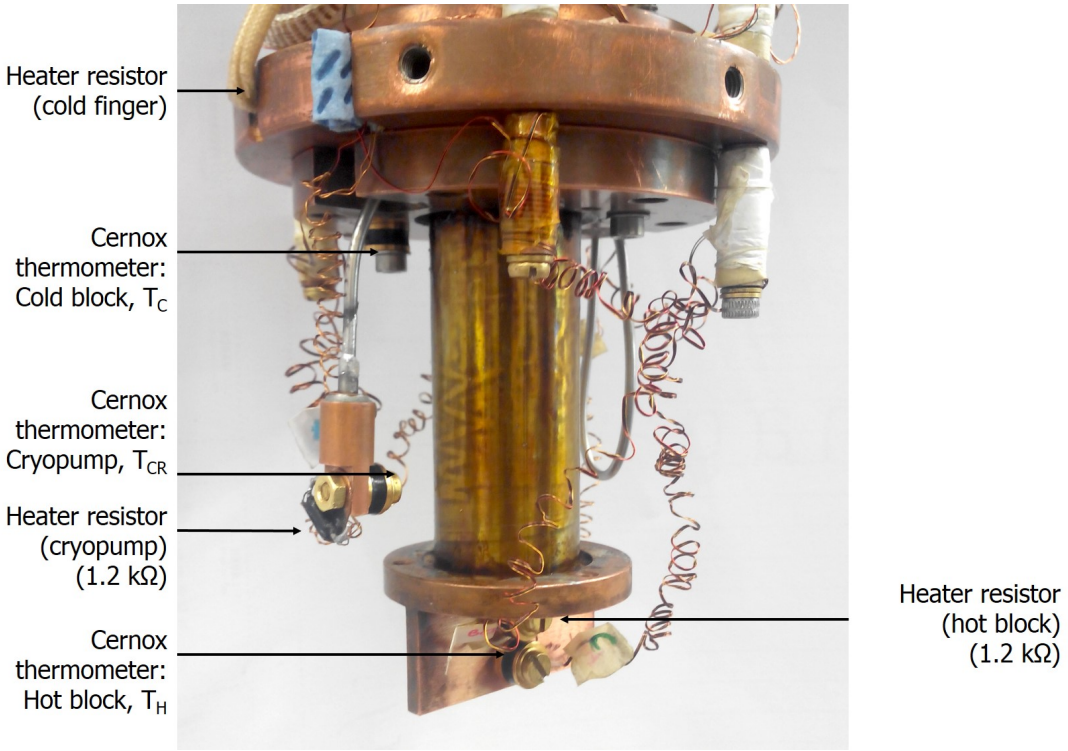

Figure 5.8: Heat switch coupled to the cold finger. The shell was covered with varnish as an attempt to repair the leaks.

5.3 Control and acquisition

The control and acquisition was adapted from a previous *LabVIEW*™ program used at this cryocooler. This program measures and shows the temperature in real time from the blocks and cryopump, its values are recorded on a data file for later analysis with *Microsoft Excel*™.

The program interacts with the temperature controller *CryoCon*™ for both the cold finger and the cryopump.

To set the heat load applied to the hot block, a voltage value was manually inserted and sent to the *Agilent*™ DC power source through the *LabVIEW*™ interface.

The *CryoCon*™ controller has also other options manageable in the *LabVIEW*™ interface, like: control the temperature of the cold finger by ramp, modify the PID values of the control loops, reading and displaying the pressure inside the switch (only for the piezoresistive sensor) are also features of the *LabVIEW*™ interface.

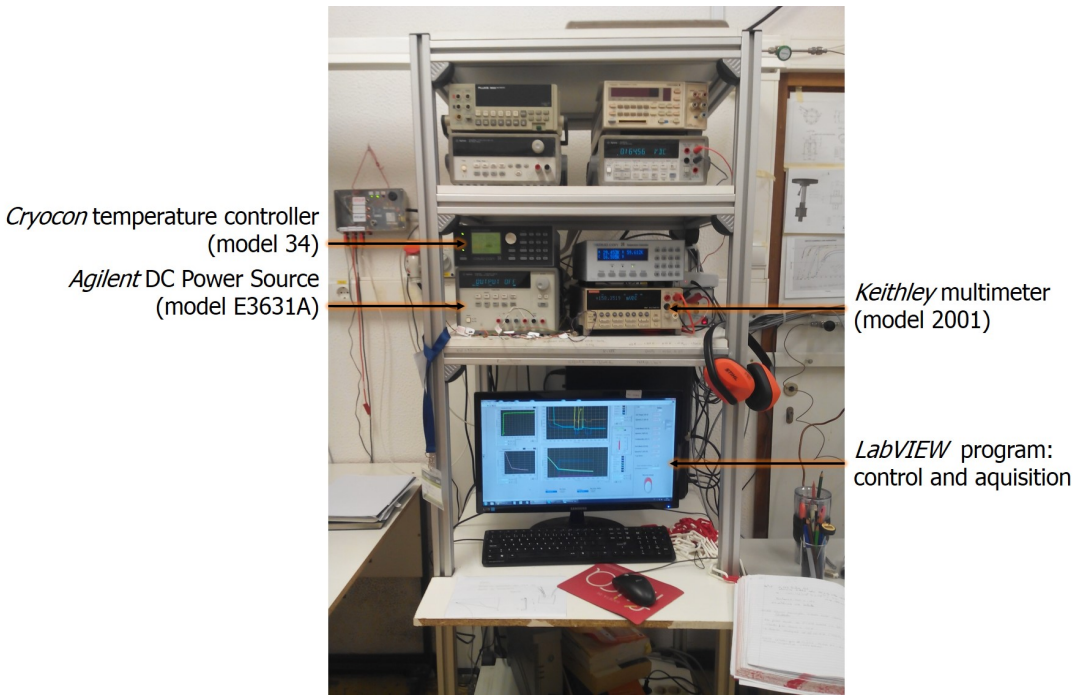

Figure 5.9: Rack with the used apparatus: temperature controller, DC power source and multimeter.

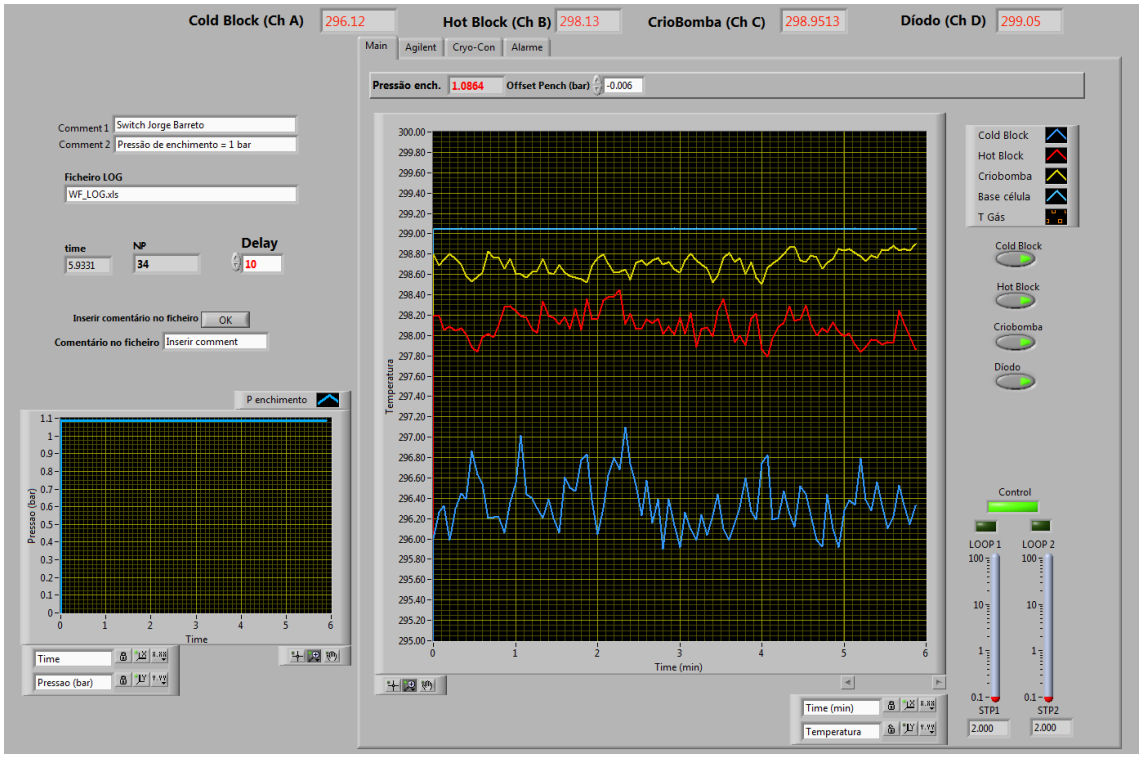

Figure 5.10: Main tab of the virtual instrument panel of the *LabVIEW*^{TM} program used in this work. This tab includes the values of the temperature, pressure and LOOP 1 & 2. The remaining tabs allows to control the loops and hot block applied power.

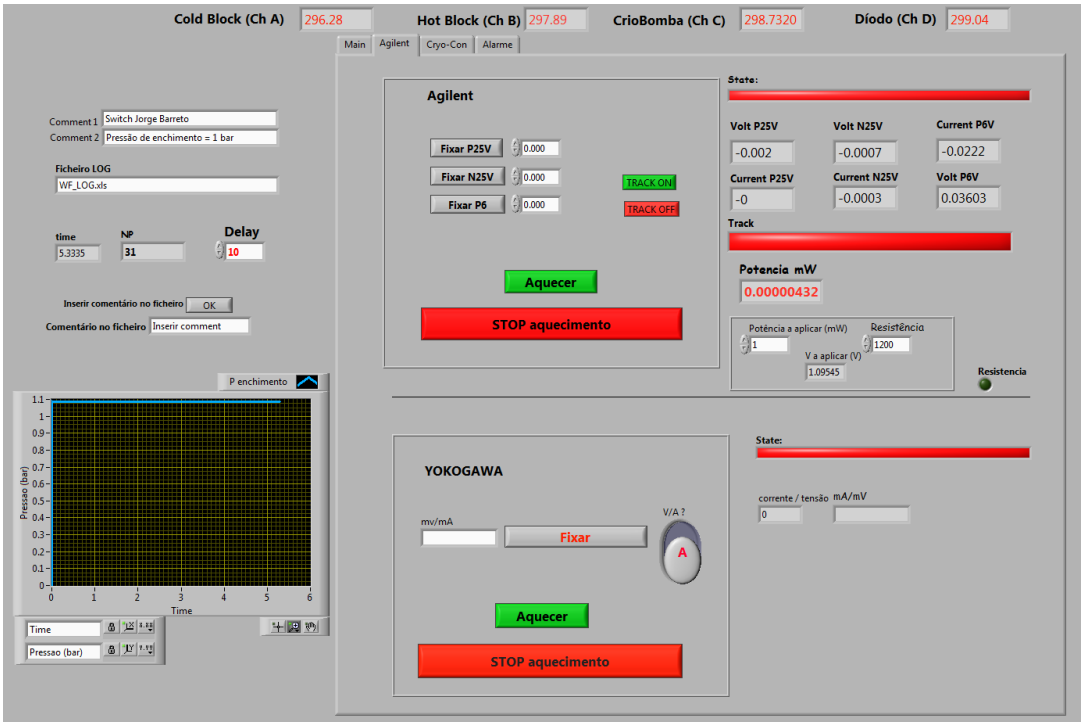

Figure 5.11: *Agilent*^{TM} tab allows to control the power applied to the hot block. The *Yokogawa*^{TM} box is disabled (not used at this work).

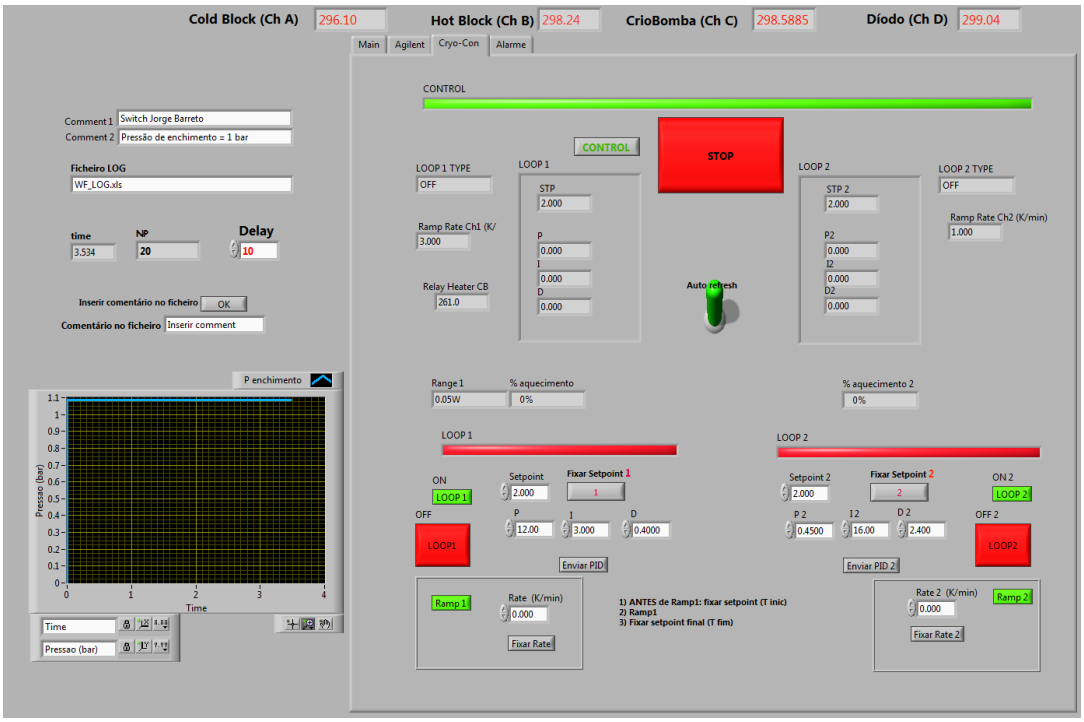

Figure 5.12: *CryoCon*™ tab allows to control the temperature of the cold finger (LOOP 1) and the cryopump (LOOP 2). The PID values can be modified at this tab. The controlled temperature is inserted at the setpoint box. It is also possible to apply a temperature ramp with the desired rate as Kelvin per minute.

CHAPTER 6

RESULTS AND DISCUSSION

6.1 ON state

The ON state with Helium-4 was characterized by applying incremental power $\dot{Q}$ to the hot block. The cold block was kept at 4 K and steady state temperature difference $\Delta T = T_{\text{hot}} - T_{\text{cold}}$ was obtained and recorded (static mode), see Fig.6.1.

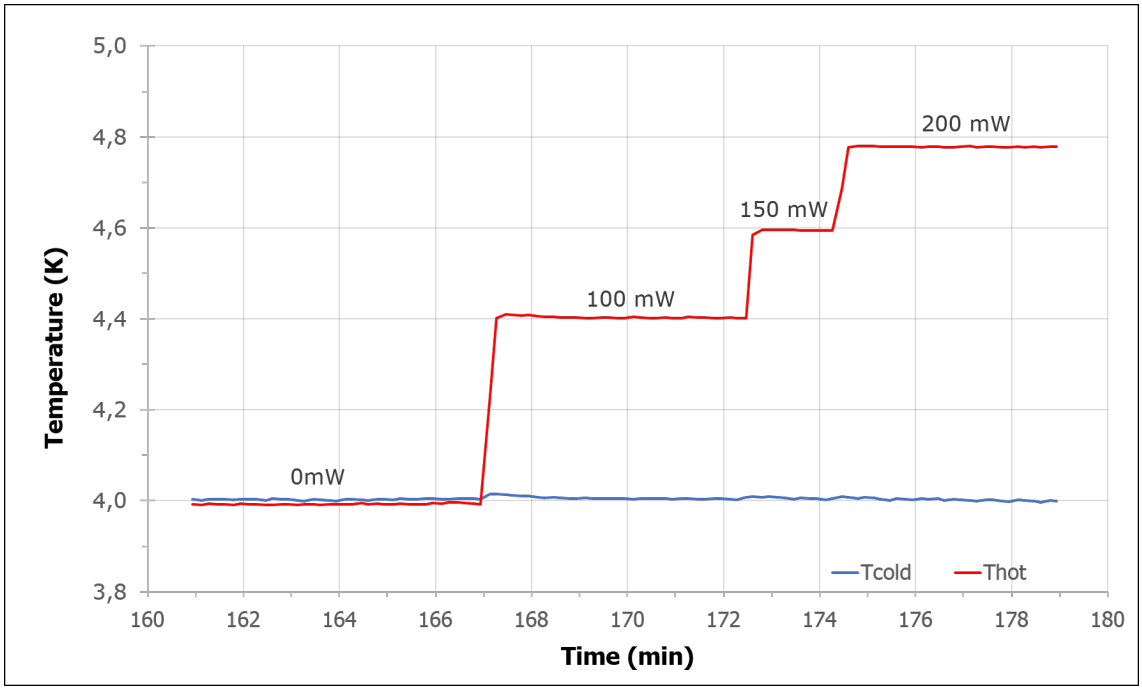

Figure 6.1: Temperature of the cold and hot blocks for different heat loads. $T_{\text{cold}} = 4$ K, sorption pump at 25 K. A stability better than 0.1 K/h was the criterion used.

As explained in section 4.4, the minimum charge pressure at room temperature to

obtain the viscous flow was $P_{\text{charge}} = 98$ mbar[1]. To guarantee no adsorption from the cryopump, this one was kept at 25 K. As for helium and activated charcoal the adsorption pump needs to be cooled down below roughly 15–20 K [7].

The heat switch was filled with Helium-4 at room temperature with different charge pressures: 12, 106 and 1000 mbar. The purpose of studying the ON state at different pressures is to demonstrate the independence of pressure at the viscous flow, only the lowest pressure was expected to show a slight smaller thermal conductance. Results are displayed in Fig.6.2.

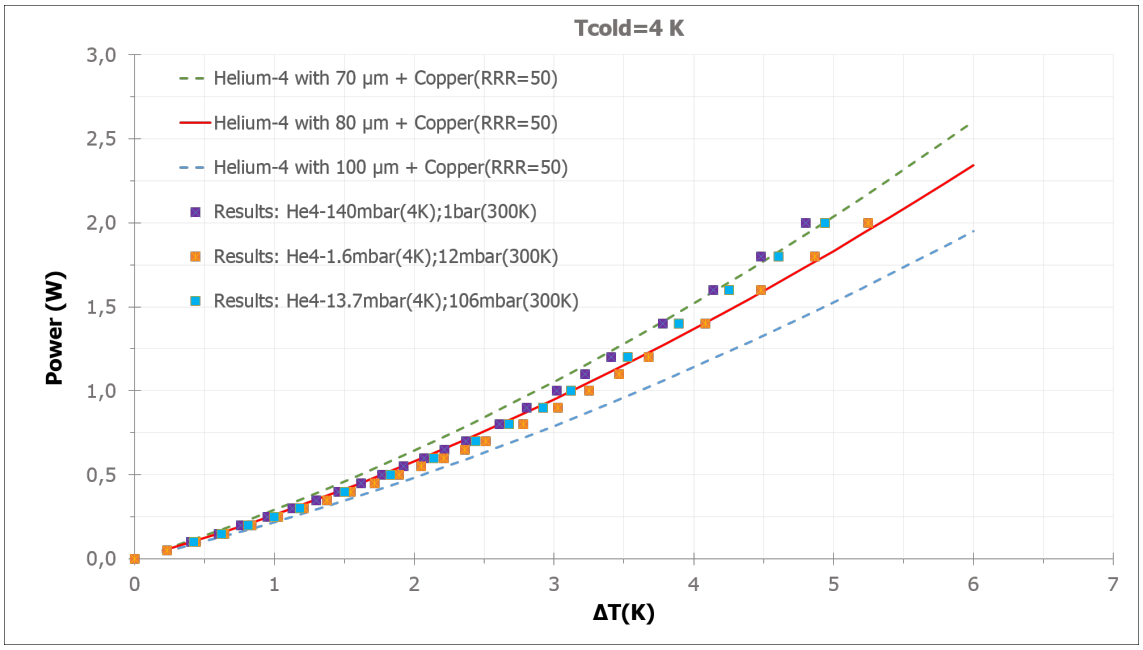

Figure 6.2: Power $\dot{Q}$ through the switch versus $\Delta T = T_{\text{hot}} - T_{\text{cold}}$ in the ON state for Helium-4 for different gap lengths and obtained experimental data. $T_c = 4$ K, sorption pump at 25 K.

When trying to fit a gap length into the thermal model by comparing with the experimental data, the expected 100 μm curve is excluded. Still, it is not possible to estimate the length of the gap at 4 K, at least one can say it is somewhat between 70 and 80 μm. The copper residual resistivity ratio (RRR) is another unknown variable, further complicating the determination of the gap.

So, to obtain the gap length the heat switch was tested with Nitrogen gas at 70 K using the same method as for Helium, the results are presented in Fig.6.3. One advantage is that the thermal conductivity of copper at 70 K it is roughly the same regardless of the purity, which does not occur at 4 K, as observed at Annex 8.3.

From Fig.6.3 the 80 μm gap curve has a very good agreement with the obtained experimental data.

[1] $P_{\text{ON}}^{\text{MIN}} = 1.3$ mbar at 4 K

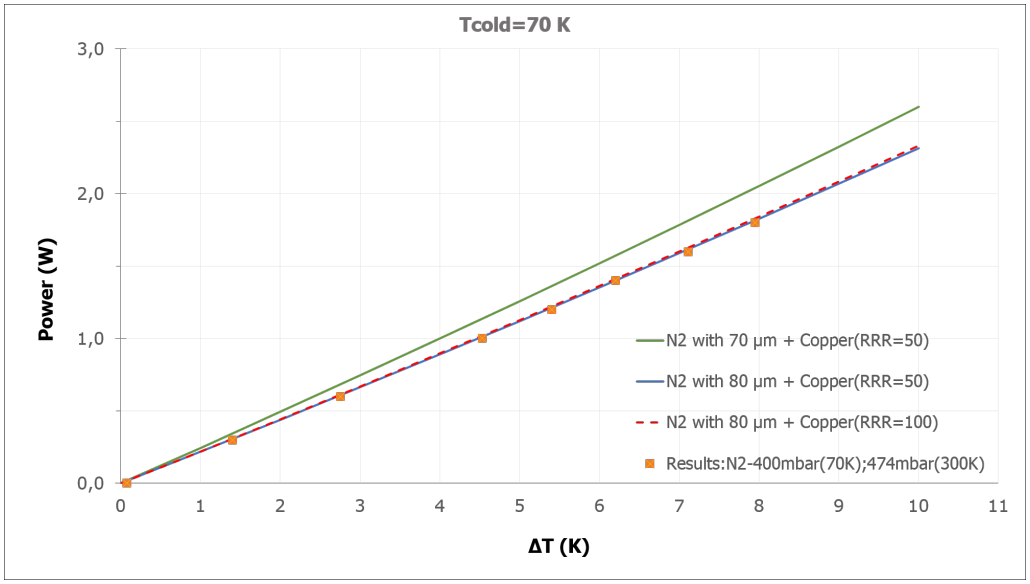

Figure 6.3: Power $\dot{Q}$ through the switch versus $\Delta T = T_{\text{hot}} - T_{\text{cold}}$ in the ON state for N_2 for different gap lengths and obtained experimental data. $T_c = 70$ K sorption pump at 140 K.

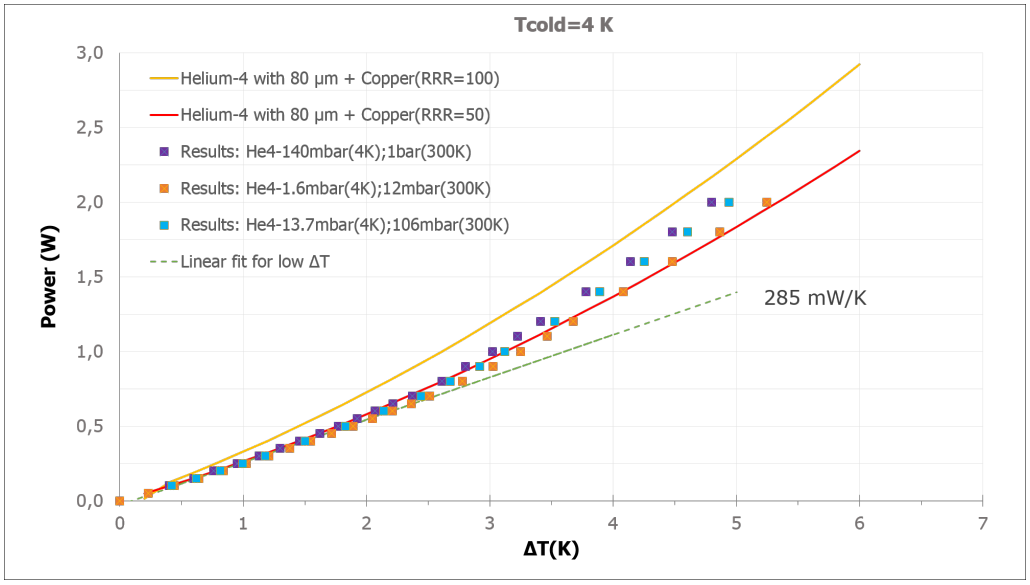

Figure 6.4: Power $\dot{Q}$ through the switch versus $\Delta T = T_{\text{hot}} - T_{\text{cold}}$ in the ON state for Helium-4. $T_c = 4$ *K*, sorption pump at 25 K.

In Fig.6.4 it is considered a gap value of 80 μm. For higher temperature differences ($\Delta T \geqslant 2$ K) the lower pressure data are not well fitted, meaning that this switch conducts better for higher pressures which is not expected from the thermal model developed. Still, the thermal conductance for low ΔT ($\leqslant 2$ K) or low power applied ($\leqslant 500$ mW) the switch thermal conductance is about 285 mW/K, as observed in the green dashed line in Fig.6.4.

The existent discrepancies may be ascribed to the copper purity. With a 80 μm gap length it was estimated from the thermal model at Fig.6.4 that the copper RRR value is between 50 and 100. A higher purity (in the considered interval) could explain the conduction for higher pressures.

Another possible justification may be ascribed to convection, which could appear at higher pressure, leading to a convective heat transfer. The *Nusselt* number is the ratio of convective to conductive heat transfer [21]. A *Nusselt* number close to one, corresponds to a pure conduction, as this number increases it corresponds to an more active convection.

$$\mathrm{Nu}_L = \frac{\text{Convective heat transfer}}{\text{Conductive heat transfer}} = \frac{hL}{k} \tag{6.1}$$

Where L is the characteristic length (gap), k is the thermal conductivity of the fluid (Helium-4), h is the convective heat transfer coefficient of the fluid. From Fig.6.4 the *Nusselt* number at $\Delta T \approx 5$ is estimated to be about 1.14. Unfortunately, no data was found for Helium-4 at 4 K regarding free convection at those pressures.

6.2 OFF state

Before testing the heat switch on the cryocooler, X-ray images were obtained at Conservation and Restoration Department at Faculdade de Ciências e Tecnologias - Universidade Nova de Lisboa to verify the correct alignment of the heat switch after assembling. Unfortunately, as observed in Fig.6.5, it was not possible to confirm the existence of the narrow gap all around between the blocks. Several X-ray images were taken for different positions, energy and exposition time, however, all of the taken images were inconclusive.

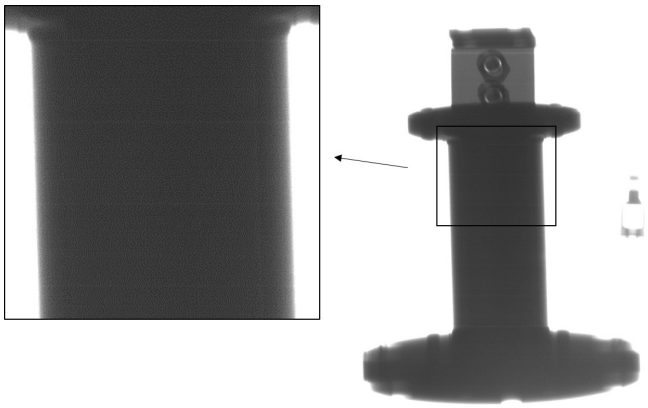

Figure 6.5: X-ray image obtained of the gas-gap heat switch.

The OFF state was also characterized by increments of power applied to the hot block with the cold block kept at 4 K. At this state the gas should be completely absorbed. Thus, no power was applied to the cryopump, reaching about 4.3 K (due to parasitical heat load) which would be sufficient to obtain a fully established OFF state.

However, the manifold adds a large hot volume to the system . About 54 cm^3 of gas (volume of the manifold + vacuum sensors) is considered to be at room temperature and only 5 cm^3 at cold temperature, the heat switch having a volume of 3.2 cm^3. Those values were obtained by a volume expansion experiment from the installed calibrated volume (1 L).

One solution is to close the valves that connect the manifold to the cryocooler (reducing the volume) or assist with another external pump, in this case the rotatory vane pump, see Figs.5.5 & 5.6, the drawback is the loss of pressure assessment.

On the first test, the switch was detached from the manifold and left open to the vacuum chamber, the vacuum was achieved by a turbo-molecular pump. The second test (when the stycast was added) the switch was connected to the manifold. Vacuum was achieved by cryo-pumping but assisted with a rotary vane pump and the cryocooler's self cryo-pumping.

The experimental data was acquired when steady state temperature difference is achieved. Due to its high thermal resistance the characteristic time of thermalization is high ($\tau_c = R_{SS}\, C$), the acquisition of each steady state takes at least 6 hours.

In order to obtain a fast acquisition, the thermal conductance can be obtained by a dynamic method. At this method the cold block is also kept at 4 K but no heat load is applied to the hot block. This one is slowly thermalized through the stainless steel shell. Known the mass of the cold block and the change in temperature of the hot block per unit time, the power through the switch is:

$$\dot{Q} = C_{\mathrm{HB}}\, \dot{T}_{\mathrm{HB}} \tag{6.2}$$

Where C_{HB} is the heat capacity of the hot block [16], $\dot{T}_{\mathrm{HB}}$ is the change in temperature of the cold block per unit time. Therefore, the cooling of the hot block was recorded as long the cold block is kept at 4 K, see Fig.6.6.

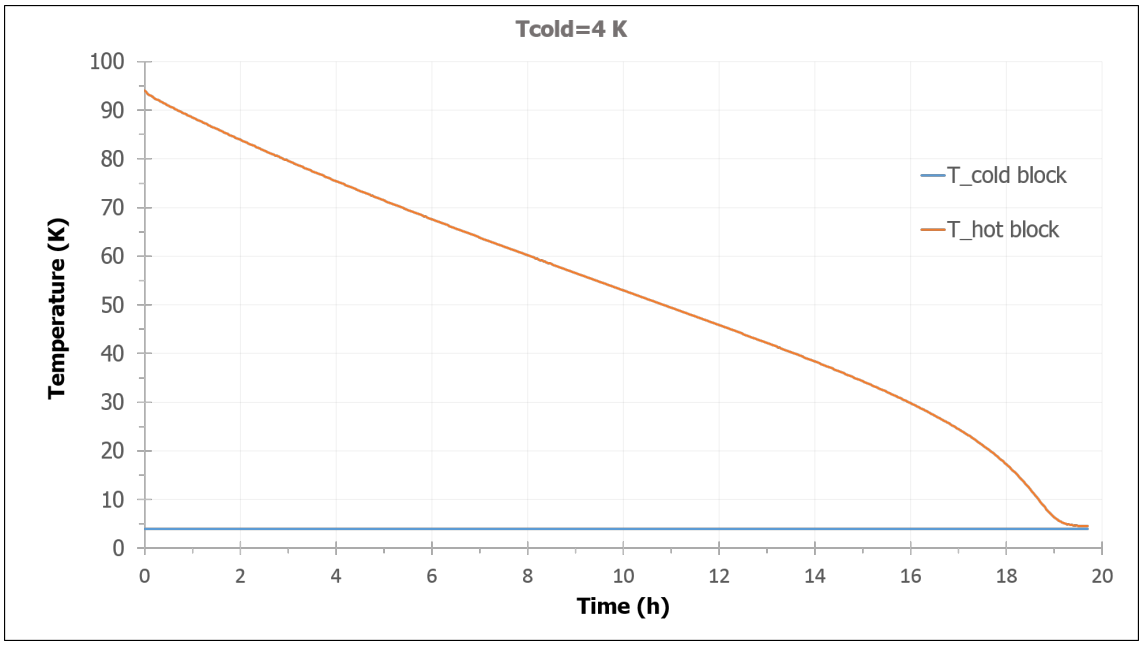

Figure 6.6: Temperature of the cold and hot blocks with no heat load applied. $T_{\mathrm{cold}} = 4$ K, sorption pump at Tsorb = 4.3 K.

From Fig.6.6 and Eq.6.2 it is obtained the thermal power as function of ΔT in the range 4-80 K. The results are shown in Fig.6.7.

The thermal model shows a good agreement with the obtained experimental data for both cases (with and without stycast).

These results allow to confirm that there is no physical contact between the blocks. Meaning that the alignment rods and soldering were successful.

The dynamic mode shows a great advantage of taking less time of acquisition and a large temperature range is characterized at once. Unfortunately, due to time and technical problems (cryo-pump is hot, no adsorption) it was not possible to obtain dynamical data for the whole all range (4-300 K).

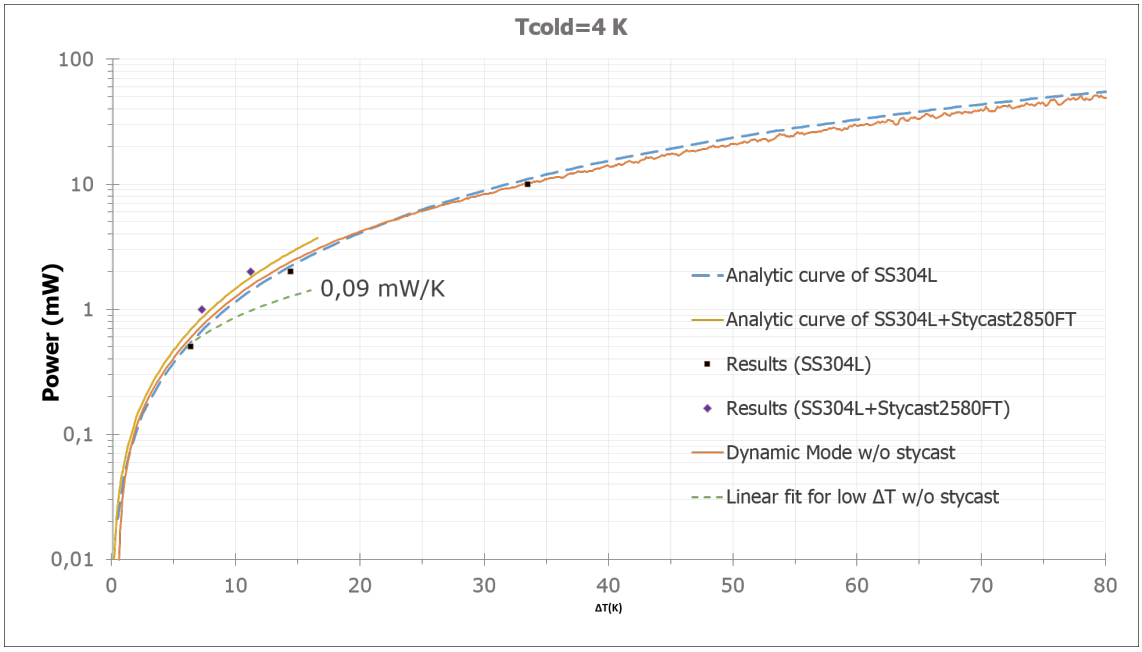

Figure 6.7: Power $\dot{Q}$ through the switch versus $\Delta T = T_{\text{hot}} - T_{\text{cold}}$ in the OFF state. $T_c = 4\ K$. Comparison between dynamic (orange line) and static mode (black data points).

It is also pointed out that the stainless steel tube length cannot be determined with accuracy, because the soldering area reduces the useful length. The stycast thickness also inserts uncertainty on the calculations. This thickness was obtained from a control sample, being estimated between 100 to 150 μm. The measurements were performed by *Mituyoyo* rugosimeter (model: Surftest SJ-210). Since the shell was covered with stycast by hand it is expected a very rough surface, so it was used the highest value obtained from the rugosimeter, (worst case scenario).

For low ΔT ($\leqslant$ 6 K) or low power applied ($\leqslant$ 1 mW) the thermal conductance is about 0.09 mW/K without stycast, as observed in the green dashed line in Fig.6.7.

Unfortunately, there was no time available to acquire data at 300 K or 436 mW (static data point). But since there is a good agreement between the analytic model and the results (static + dynamic) it can be said that, according to this model, at 300 K this switch does not conduct more than 500 mW as per requirements. Meanwhile, for the stycast, the thermal model does not include the data for all considered range, so at 300 K it is not completely secure to affirm that the switch conducts less than 500 mW, it was only found data on literature between 2.6-21 K at [19].

Also the radiation was not considered on the thermal model developed. Still, an estimative of radiative heat transfer was made a posteriori. The relationship governing the heat radiation between two hot bodies is called the Stefan-Boltzmann law:

$$\dot{Q}_{1\to 2} = \sigma A_1 F_{1\to 2}(T_1^4 - T_2^4) \tag{6.3}$$

Where σ is the Stefan–Boltzmann constant and $F_{1\to 2}$ is the view factor from surface 1

to surface 2. The view factor, for this switch between blocks corresponds to long concentric cylinders which $F_{1\to2} = 1$. Readjusting Eq.6.3 comes [21]:

$$\dot{Q}_{1\to2} = \frac{\sigma A_1 (T_1^4 - T_2^4)}{\frac{1}{\epsilon_1} + \frac{1-\epsilon_2}{\epsilon_2}\left(\frac{r_1}{r_2}\right)} \tag{6.4}$$

The emissivity of oxidated copper is between 0.5 and 0.8. Since this copper was polished and the surfaces inside the heat switch are protected from the oxygen, the emissivity falls to about 0.1 [21, 22]. Considering Eq.6.4 the radiative heat transfer comes about 75 mW at the worst case case scenario with $T_1 = 4$, $T_2 = 300$ K.

According to the analytic model the heat transfer through the shell is 436 mW. Considering now the radiation the total heat transfer is about 511 mW, which is about 2% higher than the defined limit. Still, it is an acceptable value but too close to the limit. This could be prevented by including the radiation on future versions of this analytic model used for predimensioning.

CHAPTER 7

CONCLUSION

A gas gap heat switch was studied, designed, built, assembled and tested. Its performance requirements were established as per the IUAC 4 K cryo-free magnetic properties setup.

From the developed work the gas gap heat switch prototype built with a $80\mu m$ gap length showed up two extreme thermal states. At 4 K an ON thermal conductance of 285 mW/K was obtained with Helium-4 and 0.09 mW/K at OFF (without stycast), achieving an ON/OFF ratio of 3167.

The small dimensions of the shell led to mechanical issues and a complicated assembly. Several gas leaks were detected along the shell, probably due to the complicated assembly, which could have damaged it, or thanks to the complicated mechanical construction of such a thin stainless steel shell.

The only successful solution to mask the leaks was to cover the stainless steel shell with stycast, this solution allowed to acquire experimental data without any interferences.

Without the stycast cover this heat switch would probably fit the target application. A heat transfer of 436 mW was obtained at the OFF state for the worst case scenario. But, when considering the radiation between blocks this one rises to 511 mW. Only 2% above the defined limit, however on future versions of this heat switches, the radiative heat transfer should be considered from the beginning.

There was no data found on literature on the stycast's thermal conductivity on all considered range (4-300 K), therefore it can not be guaranteed that this would fit the target application.

In order to avoid all those related problems a new model of heat switch will be developed for the cryofree project. The gas leaks probably would not exist if the shell was thicker, one solution should use a material with a lower thermal conductivity allowing to use a thicker shell.

Instead of using stainless steel, it can be used a fiberglass epoxy (G-10) which has a thermal conductivity about 10 times smaller than the stainless steel, meaning it could be

10 times thicker avoiding mechanical complications at the construction. Also the assembly would become easier, because there is no soldering involved and comes with the advantage of obtaining a clean environment inside the switch. This gas gap heat switch could be sealed like a flange type between the shell and blocks with an indium wire.

Despite all problems during the realization of this dissertation a functional switch was built , which served as a model for future applications on this cryofree project.

BIBLIOGRAPHY

[1] S Kar, P Konduru, and R Kumar. "Experimental studies on thermal behavior of 6 Tesla cryogen-free superconducting magnet system". In: *AIP Conference ...* (2012). URL: http://link.aip.org/link/?APCPCS/1434/909/1.

[2] D. G. Gilmore. *Spacecraft Thermal Control Handbook - Volume I: Fundamental Technologies*. 2002, p. 837. ISBN: 1-884989-11-X.

[3] B. Marland, D. Bugby, and C. Stouffer. "Development and testing of an advanced cryogenic thermal switch and cryogenic thermal switch test bed". In: *Cryogenics* 44.6–8 (2004). 2003 Space Cryogenics Workshop, pp. 413 –420. ISSN: 0011-2275. DOI: http://dx.doi.org/10.1016/j.cryogenics.2004.03.014. URL: http://www.sciencedirect.com/science/article/pii/S0011227504000694.

[4] G. Bonfait, I. Catarino, J. Afonso, D. Martins, M. Linder, and L. Duband. "20K Energy storage unit". In: *Cryogenics* 49 (2009), pp. 326–333. ISSN: 00112275. DOI: 10.1016/j.cryogenics.2009.03.003.

[5] I. Catarino, J. Afonso, D. Martins, M. Linder, L. Duband, and G. Bonfait. "6K solid state Energy Storage Unit". In: *Cryogenics* 50.2 (Feb. 2010), pp. 102–110. ISSN: 00112275. DOI: 10.1016/j.cryogenics.2009.12.002. URL: http://linkinghub.elsevier.com/retrieve/pii/S0011227509002021.

[6] Z. Cai, R. H. Clarke, B. A. Glowacki, W. J. Nuttall, and N. Ward. "Ongoing ascent to the helium production plateau—Insights from system dynamics". In: *Resources Policy* 35.2 (June 2010), pp. 77–89. ISSN: 03014207. DOI: 10.1016/j.resourpol.2009.10.002. URL: http://www.sciencedirect.com/science/article/pii/S0301420709000518.

[7] I. Catarino, G. Bonfait, and L. Duband. "Neon gas-gap heat switch". In: *Cryogenics* 48.1–2 (2008), pp. 17 –25. ISSN: 0011-2275. DOI: http://dx.doi.org/10.1016/j.cryogenics.2007.09.002. URL: http://www.sciencedirect.com/science/article/pii/S0011227507001233.

[8] I. Catarino and C. Paine. "3He gas gap heat switch". In: *Cryogenics* 51.1 (2011), pp. 45 –48. ISSN: 0011-2275. DOI: http://dx.doi.org/10.1016/j.cryogenics.2010.10.009. URL: http://www.sciencedirect.com/science/article/pii/S0011227510002018.

[9] K. D. Timmerhaus and T. M. Flynn. *Cryogenic process engineering*. International cryogenics monograph series. New York, NY: Plenum, 1989.

[10] C. Tantos, D. Valougeorgis, M. Pannuzzo, A. Frezzotti, and G. L. Morini. "Conductive heat transfer in a rarefied polyatomic gas confined between coaxial cylinders". In: *International Journal of Heat and Mass Transfer* 79.0 (2014), pp. 378 –389. ISSN: 0017-9310. DOI: http://dx.doi.org/10.1016/j.ijheatmasstransfer.2014.07.075. URL: http://www.sciencedirect.com/science/article/pii/S0017931014006644.

[11] D. F. Martins. "Desenvolvimento, construção e teste de um interruptor térmico para baixas temperaturas". MA thesis. Lisboa, Portugal: Universidade Nova de Lisboa, 2010.

[12] G. Ventura and L. Risegari. *The art of cryogenics: low-temperature experimental techniques*. Burlington, MA: Elsevier, 2008.

[13] T. L. Hill. *An Introduction to Statistical Thermodynamics (Dover Books on Physics)*. Dover Publications, Jan. 1987. ISBN: 0486652424. URL: http://www.worldcat.org/isbn/0486652424.

[14] C. Kittel. *Introduction to Solid State Physics*. 8th. New York: John Wiley & Sons, Inc., 2005.

[15] F. Pobell. *Matter and Methods at Low Temperatures*. 2nd. Springer, Nov. 2002. ISBN: 3540585729. URL: http://www.worldcat.org/isbn/3540585729.

[16] NIST. *Cryogenics Technologies Group*. [Online; accessed 17-July-2014]. URL: http://www.cryogenics.nist.gov/MPropsMAY/materialproperties.htm.

[17] M. M. Lemmon E.W. Huber M.L. *NIST Standard Reference Database 23: Reference Fluid Thermodynamic and Transport Properties-REFPROP*. [Version 8.0].

[18] D. Martins, L. Ribeiro, D. Lopes, I. Catarino, I. Esteves, J. Mota, and G. Bonfait. "Sorption characterization and actuation of a gas-gap heat switch". In: *Sensors and Actuators A: Physical* 171.2 (Nov. 2011), pp. 324–331. ISSN: 09244247. DOI: 10.1016/j.sna.2011.08.017. URL: http://linkinghub.elsevier.com/retrieve/pii/S0924424711004997.

[19] P. Zhang, Y. Chen, X. Ren, a.B. Wu, and Y. Zhao. "Thermal conductivity measurement of the epoxies and composite material for low temperature superconducting magnet design". In: *Cryogenics* 51.9 (Sept. 2011), pp. 534–540. ISSN: 00112275. DOI: 10.1016/j.cryogenics.2011.07.002. URL: http://linkinghub.elsevier.com/retrieve/pii/S0011227511001421.

[20] S. C. Group. *RDK-415D 4K Cryocooler Series*. [Online; accessed 10-08-2014]. URL: http://www.shicryogenics.com/products/4k-cryocoolers/rdk-415d-4k-cryocooler-series/.

[21] F. P. Incropera. *Fundamentals of Heat and Mass Transfer*. John Wiley & Sons, 2006. ISBN: 0470088400.

[22] J. Franco. "Interruptor térmico criogénico a gás de troca com hiato obtido por dilatação diferencial". MA thesis. Universidade Nova de Lisboa, 2011. URL: http://run.unl.pt/handle/10362/6629.

[23] Lakeshore. *Appendix I: Cryogenic Reference Tables*. [Online; accessed 16-07-2014]. URL: http://www.lakeshore.com/Documents/LSTC_appendixI_l.pdf.

[24] B. N. laboratory database. *Materials database: Coppers*. [Online; accessed 11-09-2014]. URL: http://materialdatabase.magnet.fsu.edu/Copper.htm.

CHAPTER 8

ANNEXES

8.1 Thermal conductivity integral of selected materials

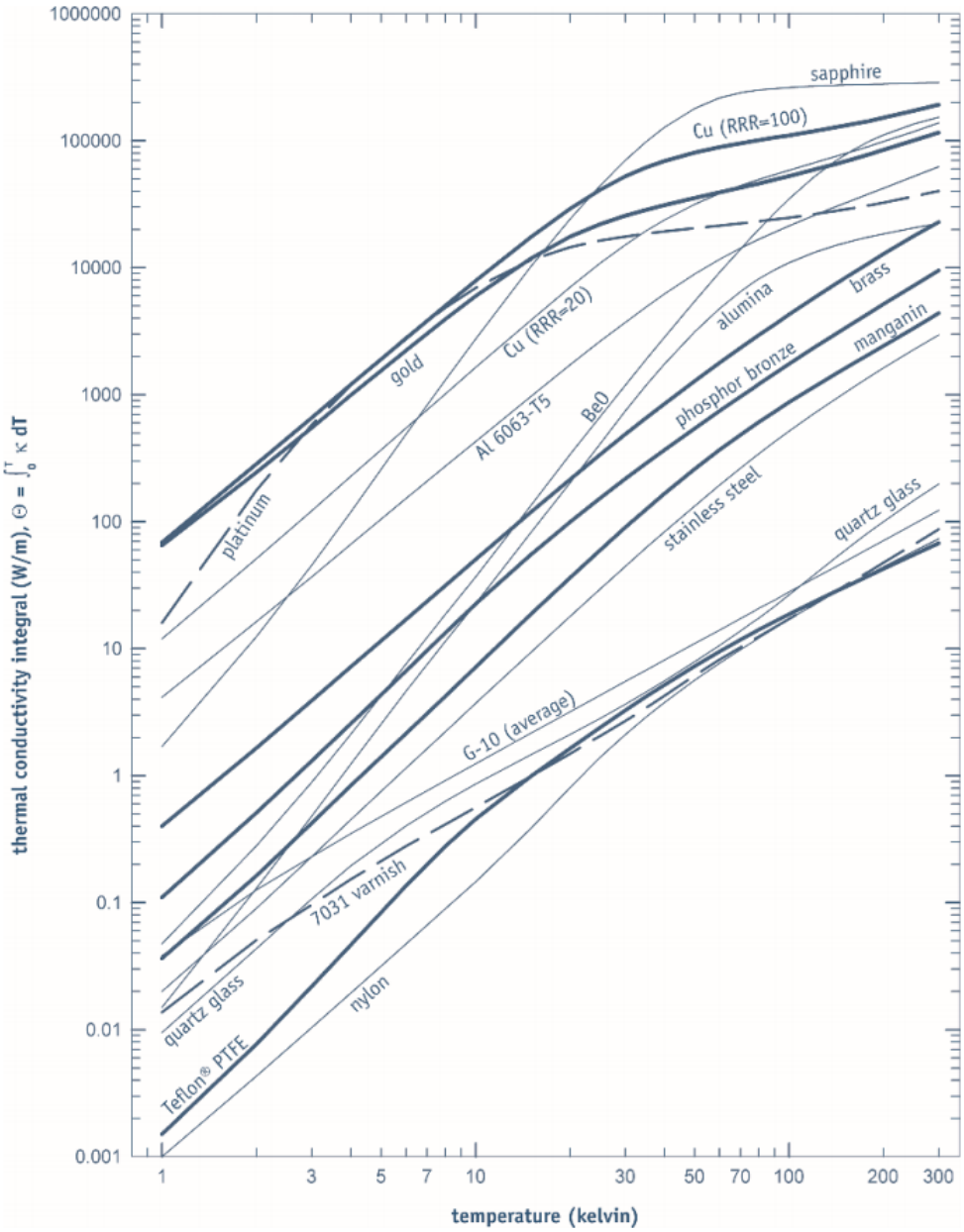

Figure 8.1: Integral thermal conductivity integral of selected materials (in W/m) [23].

8.2 RDK-415D cold head capacity map

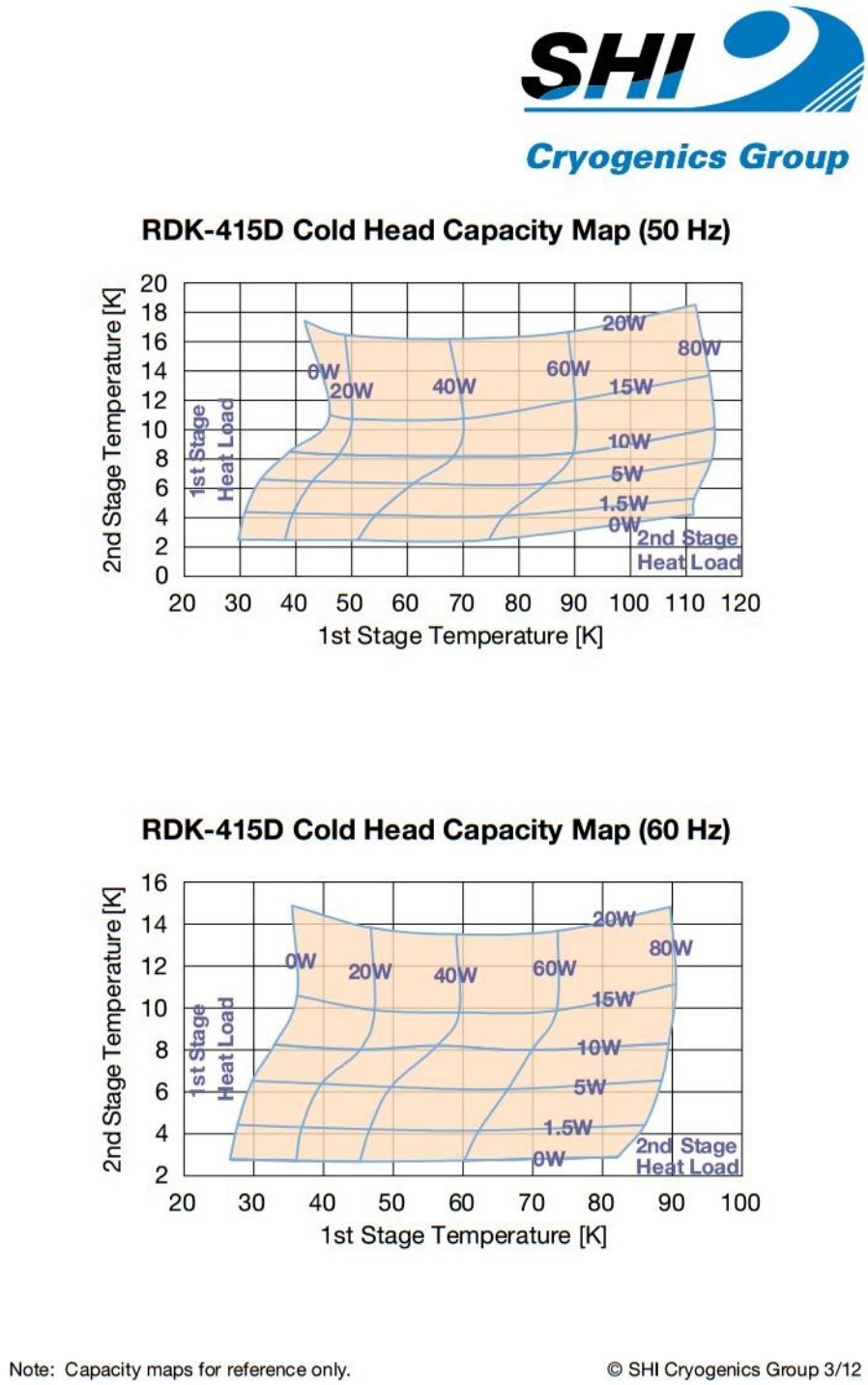

Figure 8.2: RDK-415D cold head capacity map for 50 and 60 Hz [20].

8.3 Thermal conductivity of copper

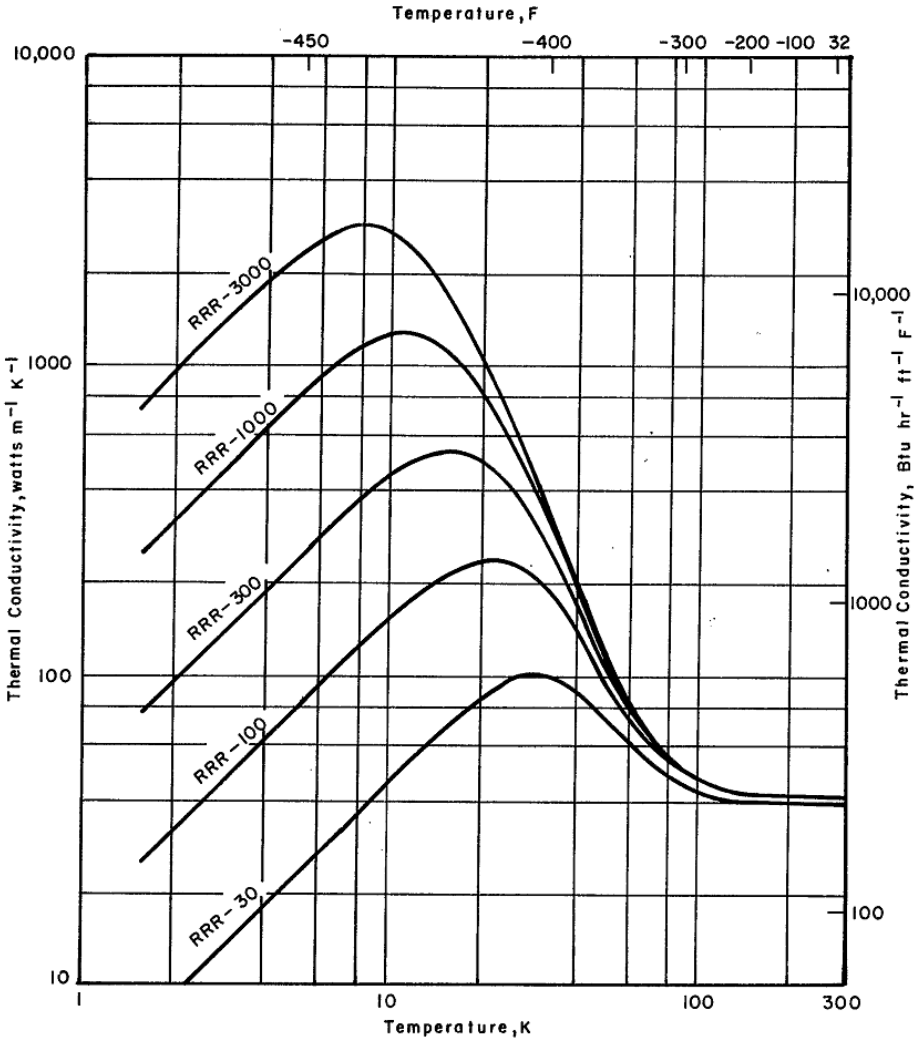

Figure 8.3: Thermal conductivity of copper [24].

CHAPTER 9

APPENDICES

9.1 Technical drawings

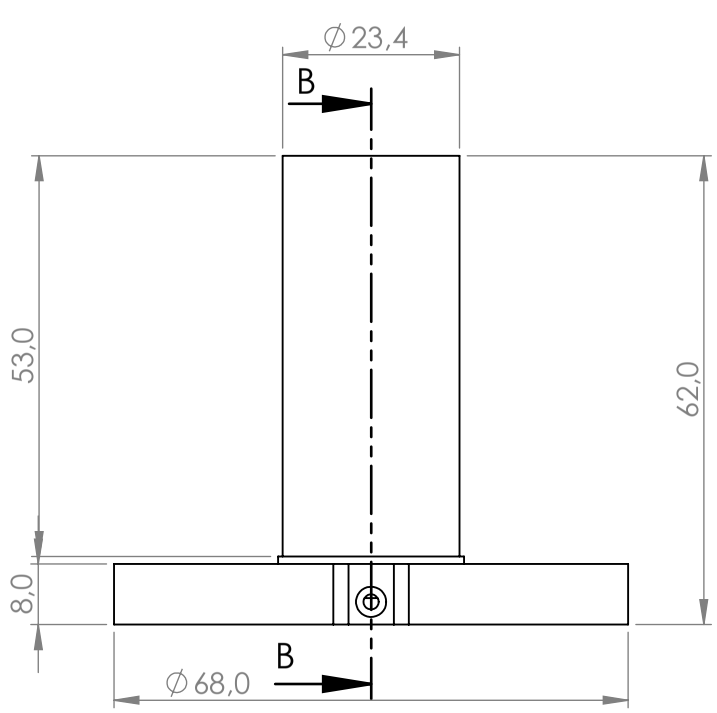

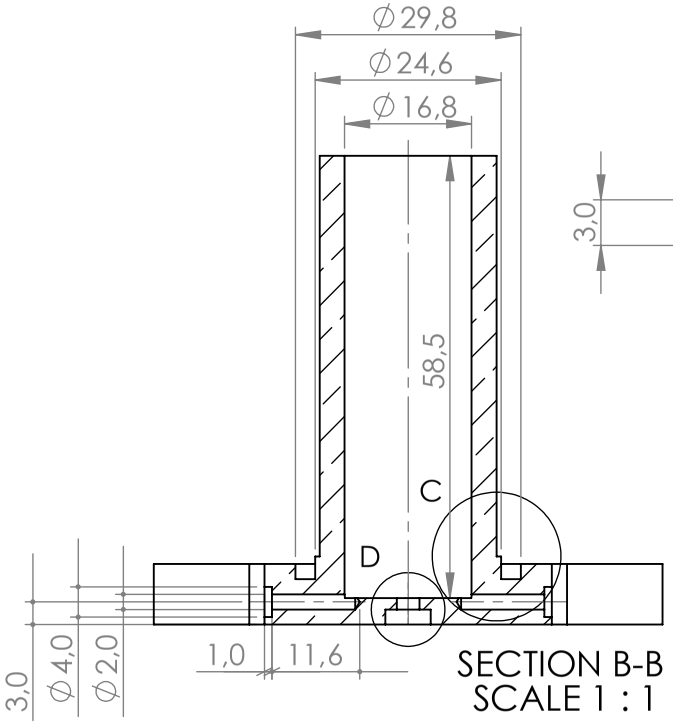

SECTION B-B
SCALE 1 : 1

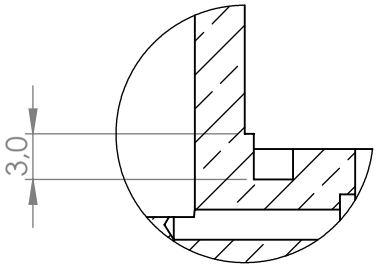

DETAIL C
SCALE 2 : 1

FIRST ANGLE PROJECTION

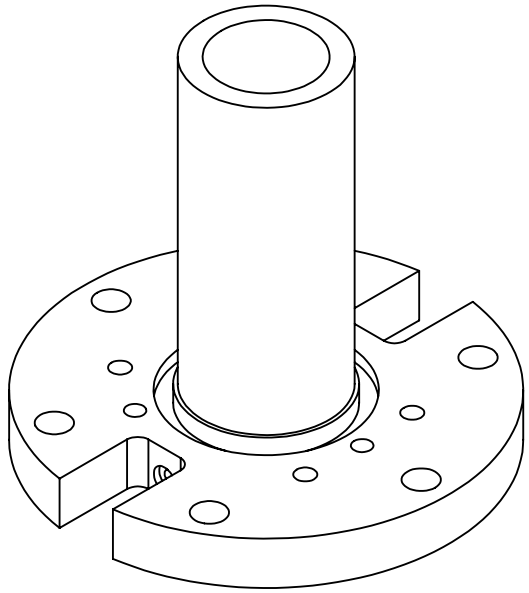

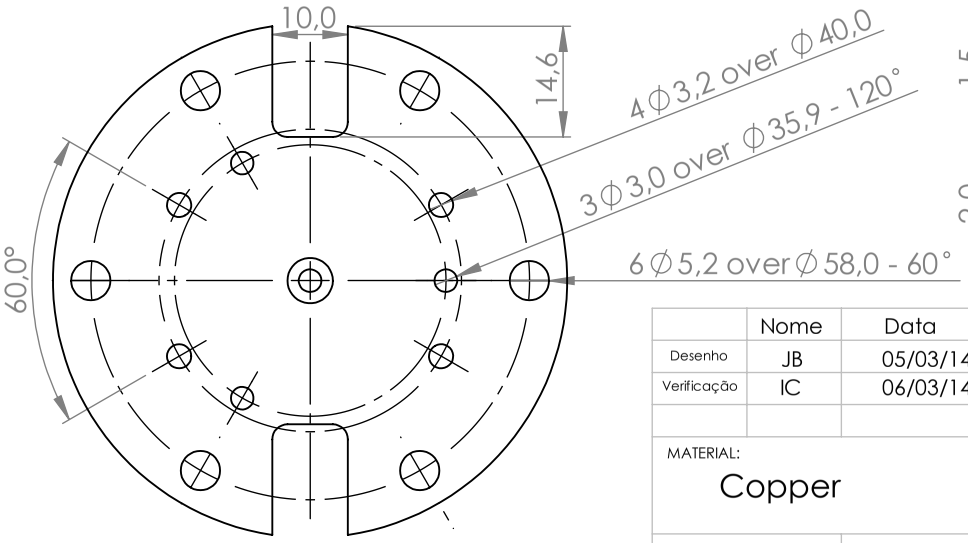

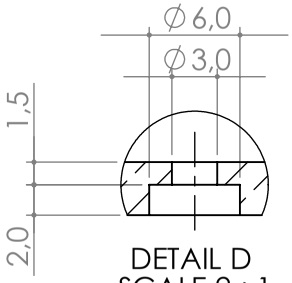

DETAIL D
SCALE 2 : 1

	Nome	Data
Desenho	JB	05/03/14
Verificação	IC	06/03/14

MATERIAL:
Copper

Peça:
Cold Block

Lab. Criogenia FCT-UNL

Tamanho: A4
Escala: 1: 1

Tolerância:
X: ±0.1

Nome desenho:
Copper cold block

1 peça

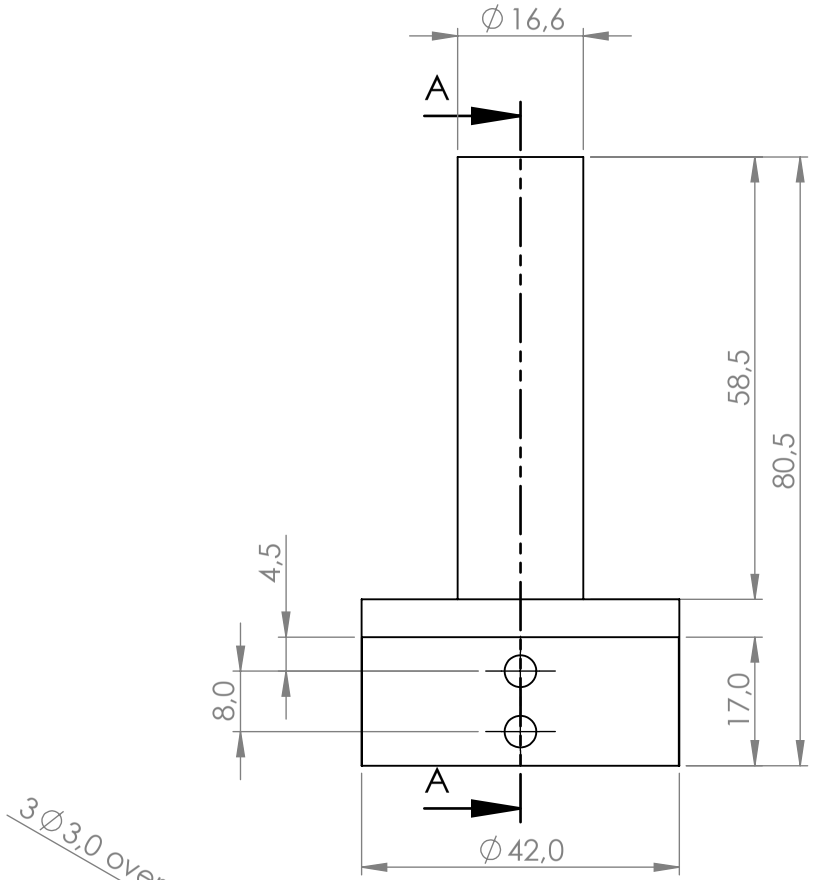

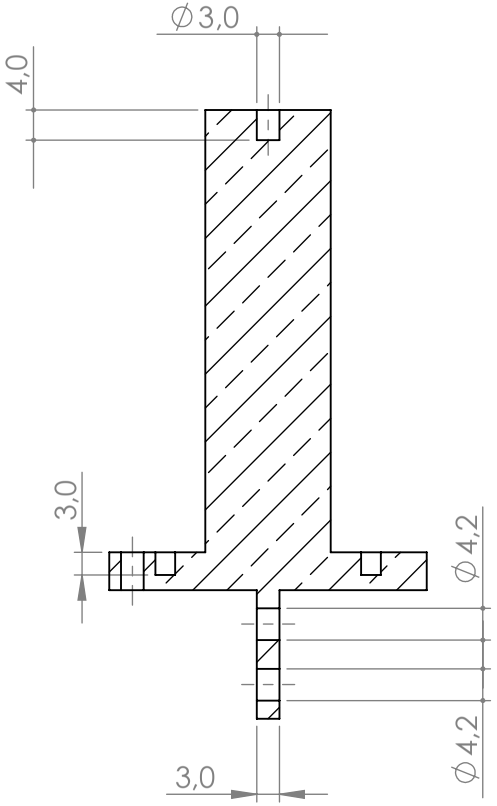

SECTION A-A
SCALE 1 : 1

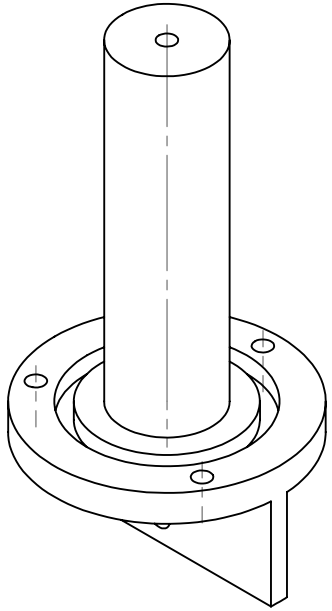

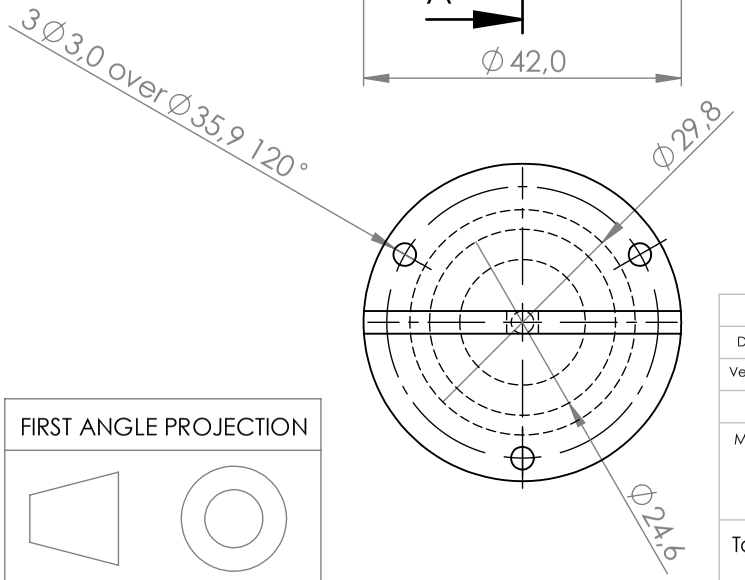

FIRST ANGLE PROJECTION

	Nome	Data
Desenho	JB	05/03/14
Verificação	IC	06/03/14

MATERIAL: Copper

Peça: **Hot Block**

Lab. Criogenia FCT-UNL

Tamanho: A4

Escala: 1:1

Tolerância: X:±0.1

Nome desenho: Copper hot block

1 peça

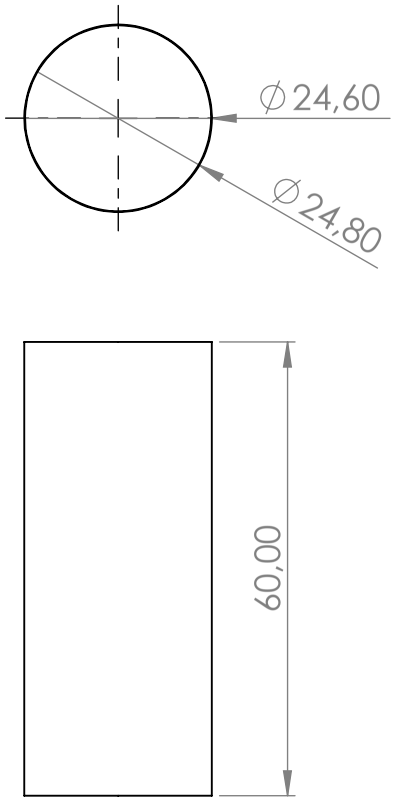

	Nome	Data
Desenho	JB	03/03/14
Verificação	IC	06/03/14	

Peça:

Stainless Steel Shell

Lab. Criogenia FCT-UNL

FIRST ANGLE PROJECTION

MATERIAL:

SS304L

Tamanho: A4

Escala: 1: 1

Tolerância:

X: ±0.01

Nome desenho:

Stainless steel support shell

1 peça

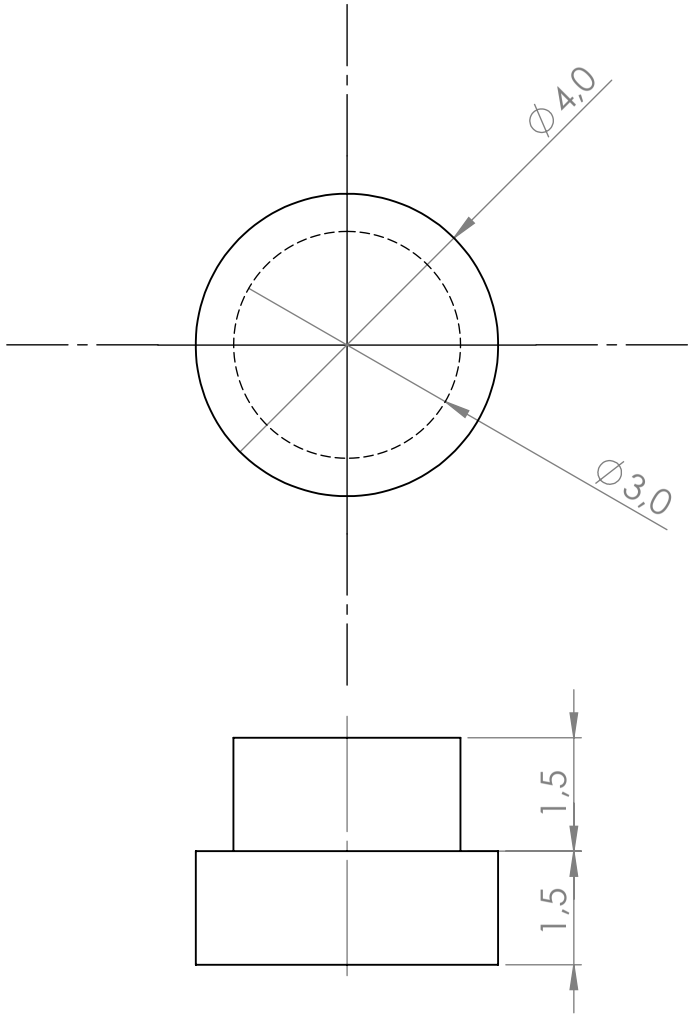

FIRST ANGLE PROJECTION

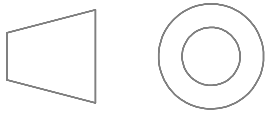

	Nome	Data
Desenho	JB	28/04/14
Verificação	IC	28/04/14

MATERIAL: Copper

Peça: **Stopper**

Lab. Criogenia FCT-UNL

Tamanho: A4

Escala: 10: 1

Tolerância: X: ±0.1

Nome desenho: Copper stopper (for cold block)

1 peça